Grain Yield Observations Constrain Cropland CO2 Fluxes Over Europe

Combe, M.; de wit, Allard J. W.; de Arellano, J. Vila-Guerau; van der Molen, M. K.; Magliulo, V.; Peters, W.

Published in:
Journal of geophysical research-Biogeosciences

DOI:
10.1002/2017JG003937

AGU PUBLICATIONS

JGR

Journal of Geophysical Research: Biogeosciences

RESEARCH ARTICLE
10.1002/2017JG003937

Grain Yield Observations Constrain Cropland CO_2 Fluxes Over Europe

M. Combe[1], A. J. W. de Wit[2], J. Vilà-Guerau de Arellano[3], M. K. van der Molen[3], V. Magliulo[4], and W. Peters[3,5]

[1]CAVElab Computational and Applied Vegetation Ecology, Department of Applied Ecology and Environmental Biology, Faculty of Bioscience Engineering, Ghent University, Ghent, Belgium, [2]Earth Observation and Environmental Informatics, Alterra Wageningen UR, Wageningen, Netherlands, [3]Department of Meteorology and Air Quality, Wageningen University, Wageningen, Netherlands, [4]ISAFoM-Institute for Mediterranean Agricultural and Forest Systems, National Research Council, Ercolano, Italy, [5]Centre for Isotope Research, University of Groningen, Groningen, Netherlands

Key Points:
- We present a novel framework to constrain cropland CO_2 exchange in Europe from crop yield observations
- It gives a realistic estimate of daily and seasonal cropland carbon fluxes compared to independent measurements and biosphere models
- Local information on sowing, irrigation, and harvesting dates could help to improve it, as well as improved modeling of soil moisture stress

Correspondence to:
M. Combe,
marie.combe@ugent.be

Citation:
Combe, M., de Wit, A. J. W., Vilà-Guerau de Arellano, J., van der Molen, M. K., Magliulo, V., & Peters, W. (2017). Grain yield observations constrain cropland CO_2 fluxes over Europe. *Journal of Geophysical Research: Biogeosciences*, *122*, 3238–3259. https://doi.org/10.1002/2017JG003937

Received 12 MAY 2017
Accepted 10 OCT 2017
Accepted article online 18 OCT 2017
Published online 23 DEC 2017

Abstract Carbon exchange over croplands plays an important role in the European carbon cycle over daily to seasonal time scales. A better description of this exchange in terrestrial biosphere models—most of which currently treat crops as unmanaged grasslands—is needed to improve atmospheric CO_2 simulations. In the framework we present here, we model gross European cropland CO_2 fluxes with a crop growth model constrained by grain yield observations. Our approach follows a two-step procedure. In the first step, we calculate day-to-day crop carbon fluxes and pools with the WOrld FOod STudies (WOFOST) model. A scaling factor of crop growth is optimized regionally by minimizing the final grain carbon pool difference to crop yield observations from the Statistical Office of the European Union. In a second step, we re-run our WOFOST model for the full European 25 × 25 km gridded domain using the optimized scaling factors. We combine our optimized crop CO_2 fluxes with a simple soil respiration model to obtain the net cropland CO_2 exchange. We assess our model's ability to represent cropland CO_2 exchange using 40 years of observations at seven European FluxNet sites and compare it with carbon fluxes produced by a typical terrestrial biosphere model. We conclude that our new model framework provides a more realistic and strongly observation-driven estimate of carbon exchange over European croplands. Its products will be made available to the scientific community through the ICOS Carbon Portal and serve as a new cropland component in the CarbonTracker Europe inverse model.

1. Introduction

Even though croplands occupy about 12% of the Earth land surface (1990s estimate from Ramankutty et al., 2002), they are usually considered not to contribute to the global land carbon sink (see the neutral balance assumption in Smith et al., 2014, or Gray et al., 2014). This neutral contribution is justified by a lack of long-term carbon storage in crop biomass and in intensely used agricultural soils (Lal, 2004), in contrast to forests (Pan et al., 2011). Crop harvests are rapidly consumed, their residues are incorporated into the cropland soils, and thus, most of their stored carbon is respired back into the atmosphere within a few years. However, seasonally, crop productivity still strongly impacts measured atmospheric CO_2 concentrations.

Croplands have a different seasonal cycle compared to natural vegetation, their seasonal CO_2 uptake being shorter in time and larger in magnitude (Corbin et al., 2010). It is thus understandable that they strongly impact measured CO_2 concentrations locally (Tolk et al., 2009). Recently, Gray et al. (2014) and Zeng et al. (2014) have also shown that the footprint of croplands can be found in the 25% increase in the seasonal amplitude of atmospheric CO_2 over remote and naturally vegetated sites. This increase can be explained by the 200% rise in crop productivity since the green revolution (Pingali, 2012), a trend that is likely to continue as roughly 9 billion people are expected to be fed by agriculture by 2050 (Roberts, 2011). Given the large impact of cropland CO_2 exchange on atmospheric CO_2 mole fractions on daily to seasonal scales, croplands CO_2 exchange must be properly represented in atmospheric CO_2 models and coupled carbon-climate models. Proper representation of this short-term cropland CO_2 exchange should furthermore help to reduce the uncertainty in inverse model estimates of the total land carbon sink, the most variable and uncertain sink of the global carbon budget (Le Quéré et al., 2015).

To model land surface CO_2 exchange, a vast majority of terrestrial biosphere models (TBMs) use the concept of plant functional type (PFT). TBMs with PFTs simplify croplands as unmanaged grassland in a unique PFT or go as far as separating it into two types for C_3 and C_4 photosynthesis (e.g., the ORCHIDEE model in Krinner et al., 2005). Over croplands, all PFT models neglect the effect of key processes such as crop phenology (the timing of crop maturation), crop management (tillage, irrigation, fertilization, etc.), or the lateral transport of carbon after the harvest. Efforts to include such crop-specific processes (Lokupitiya et al., 2016; Wu et al., 2016) and crop-specific values for photosynthesis parameters (Kothavala et al., 2005) in TBMs have shown major improvements in the daily to interannual variability of cropland surface carbon and water exchange. When absent from model formulation, data assimilation can alternatively successfully constrain some of those processes (e.g., phenology with remotely sensed vegetation greenness, see Sus et al., 2013). We argue that the integration of both crop-specific models—which can represent species-dependent crop processes—and of systematic observations performed over croplands could help make efficient simulations of cropland carbon cycling. The effectiveness of such novel model-data integration approaches for modeling cropland CO_2 exchange then needs to be evaluated, for instance, using readily available networks of eddy-covariance data (Ciais et al., 2010).

In this study, we aim to improve the simulation of the diurnal to seasonal cropland carbon exchange over Europe in a novel way. In contrast to more classical approaches that usually aim at extending TBM formulations (e.g., Lokupitiya et al., 2009), our strategy is to use an existing stand-alone crop growth model to simulate cropland CO_2 exchange and to constrain it with observations of grain yield. For this, we use the WOFOST-WLP model (Supit et al., 1994), which computes the daily water-limited photosynthesis, autotrophic and maintenance respiration fluxes, crop phenology, and crop yield. We assimilate grain yield observations from the Statistical Office of the European Union (EUROSTAT, 2015) to constrain crop productivity and bring it from the modeled water-limited to the actual crop production level. By optimizing crop growth, we hence intend to indirectly represent all nonmodeled growth processes (mostly fertilization, pests, and diseases). We then combine the WOFOST model results with a soil respiration function that depends on temperature to obtain the net surface CO_2 exchange over croplands. We finally evaluate our CO_2 exchange product against independent observations of surface CO_2 fluxes from the FluxNet community (Baldocchi et al., 2001). To our knowledge, we become the first to use the readily available grain yield stream of data to constrain a model for cropland net CO_2 exchange, useful to the biogeosciences and atmospheric sciences. Our modeling framework makes moreover use of a complete database for European crop calendars, crop species, and a detailed European soil map (Boogaard et al., 2013). It is operational for the European domain, for the ten most grown crop species, and has a spatial resolution of 25 km.

We use our novel model-data integration framework—which we hereafter refer to as WOFOST-opt—to address three research questions:

1. How well can WOFOST-opt reproduce the cropland photosynthesis and respiration fluxes in Europe, this from the daily to the seasonal scales?
2. To what extent does the integration of yield data constrain the WOFOST-opt net cropland CO_2 exchange (i.e., NEE)?
3. Can our framework capture cropland NEE during agricultural droughts?

With these research questions, we thus address the performance of our framework under normal to water-limiting conditions. We first answer research questions 1 and 2 by comparing our CO_2 exchange product to independent observations from the FluxNet community (Baldocchi et al., 2001) and also to crop simulations by the PFT-based TBM SiBCASA (van der Velde, 2015), at seven cropland sites across Europe located within three contrasting climate zones. Together, this comparison covers 40 site years of observations and model. We then answer our third research question by modeling the total cropland CO_2 exchange during the 2005 drought over the Iberian peninsula, and by analyzing the effect of water stress on the net cropland CO_2 exchange. We finally discuss the capacity of our methodology to produce high-resolution hindcasts of cropland CO_2 exchange, and their utility as boundary conditions in atmospheric models used for European carbon cycle studies.

2. Model Description

2.1. Crop Photosynthesis and Respiration

We use the WOrld FOod STudies water-limited production model (WOFOST-WLP) version 7.1 to represent the crop gross primary production (GPP) and autotrophic respiration (R_{aut}) during the growing season. WOFOST is an agricultural crop growth model from the Wageningen school of models (Supit et al., 1994; van Ittersum et al., 2003). Its original purpose is to compute crop yields (i.e., the accumulation of carbon in the grains or tubers of the plant). To do this, WOFOST models the crop CO_2 exchange with the atmosphere on a daily time step. Note that the atmosphere is not coupled to the vegetation but treated here as a boundary condition: six weather variables (the incoming short-wave radiation, minimum and maximum air temperature, atmospheric vapor pressure, precipitation, and wind speed) are provided every day as input to the crop photosynthesis and respiration models (see section 3.1). The model then recreates a diurnal cycle for radiation and temperature only, assuming a Gaussian distribution.

WOFOST calculates the instantaneous gross assimilation rate of a leaf layer ($A_l(z,t)$, in $kg_{CO_2}\ ha_{leaf}^{-1}\ h^{-1}$) using a two big-leaf light-use efficiency approach:

$$\begin{aligned} A_{\text{sha}}(z,t) &= A_m \left(1 - e^{-\varepsilon \frac{\text{PAR}_{a,\text{sha}}}{A_m}}\right), \\ A_{\text{sun}}(z,t) &= A_m \left\{1 - \frac{(A_m - A_{\text{sha}})}{\varepsilon \times \text{PAR}_{a,\text{sun}}} \times \left(1 - e^{-\varepsilon \frac{\text{PAR}_{a,\text{sun}}}{A_m}}\right)\right\}, \\ A_l(z,t) &= f_{\text{sun}}\, A_{\text{sun}} + (1 - f_{\text{sun}})\, A_{\text{sha}}, \end{aligned} \tag{1}$$

with z the height of the leaf layer, t the time in hours, A_{sha} and A_{sun}, respectively, the instantaneous gross assimilation rates of shaded and sunlit leaves, A_m the maximum leaf assimilation rate at light saturation that is dependent on the air temperature and the development stage of the crop, ε the light-use efficiency in $kg_{CO_2}\ ha_{leaf}^{-1}\ hr^{-1}/(W\ m^{-2})$, $\text{PAR}_{a,\text{sha}}$ and $\text{PAR}_{a,\text{sun}}$ the amount of photosynthetically active radiation absorbed by respectively the shaded and the sunlit part of the leaf layer in $W\ m^{-2}$, and f_{sun} the fraction of sunlit leaf area. Within the canopy, A_l varies along height due to the extinction of light caused by the leaves self-shading, and along time following the diurnal course of radiation and temperature. We upscale A_l to its canopy level (A_c, in $kg_{CO_2}\ ha_{ground}^{-1}\ h^{-1}$) with a Gaussian integration (Scheid, 1968) of A_l over three leaf layers (z_0, z_1, and z_2):

$$A_c(t) = \int_{z=0}^{z_{\text{top}}} A_l(z,t)\ \text{d}z \ \approx\ \text{LAI} \times \frac{A_l(z_0,t) + 1.6\,A_l(z_1,t) + A_l(z_2,t)}{3.6}, \tag{2}$$

with LAI the leaf area index in $ha_{leaf}\ ha_{ground}^{-1}$. We then compute the daily potential canopy GPP (GPP_p, in $kg_{CO_2}\ ha_{ground}^{-1}\ d^{-1}$, also see Figure 1) with the same Gaussian integration approach over three points in time selected from noon to sunset (t_0, t_1, and t_2):

$$\text{GPP}_p = -\int_{t=\text{sunrise}}^{t=\text{sunset}} A_c(t)\ \text{d}t \ \approx\ -I_{\text{day}} \times \frac{A_c(t_0) + 1.6\,A_c(t_1) + A_c(t_2)}{3.6}, \tag{3}$$

with I_{day} the day length in hours. Note that we adopt hereafter a sign convention where carbon fluxes are seen from the perspective of the atmosphere, hence the added negative sign in equation (3).

We then account for the effect of (a) water stress and (b) all other limitations to growth (e.g., weeds, pests, and diseases) by multiplying GPP_p with two empirical factors: (*a*) a water-stress factor (f_{stress}) that varies in time following the amount of available soil moisture and (*b*) a fixed yearly yield gap factor (f_{gap}) that is based on observations of crop yields and that allows us to regulate the modeled crop production further down to its actual level. We obtain the actual canopy GPP (in $g_C\ m^{-2}\ d^{-1}$) with the following expression:

$$\text{GPP} = \text{GPP}_p \times C_e \times f_{\text{stress}} \times f_{\text{gap}}, \tag{4}$$

with C_e the conversion factor of $kg_{CO_2}\ ha^{-1}$ to $g_C\ m^{-2}$, and both f_{stress} and f_{gap} dimensionless and ranging from 0 to 1. We explain the computation of f_{stress} and f_{gap}, respectively, in sections 2.2 and 3.2. When applying equation (4), it is important to realize that the yearly value of f_{gap} scales down crop growth as well as the coupled evapotranspiration, which interacts with the evolution of f_{stress} along the growing season.

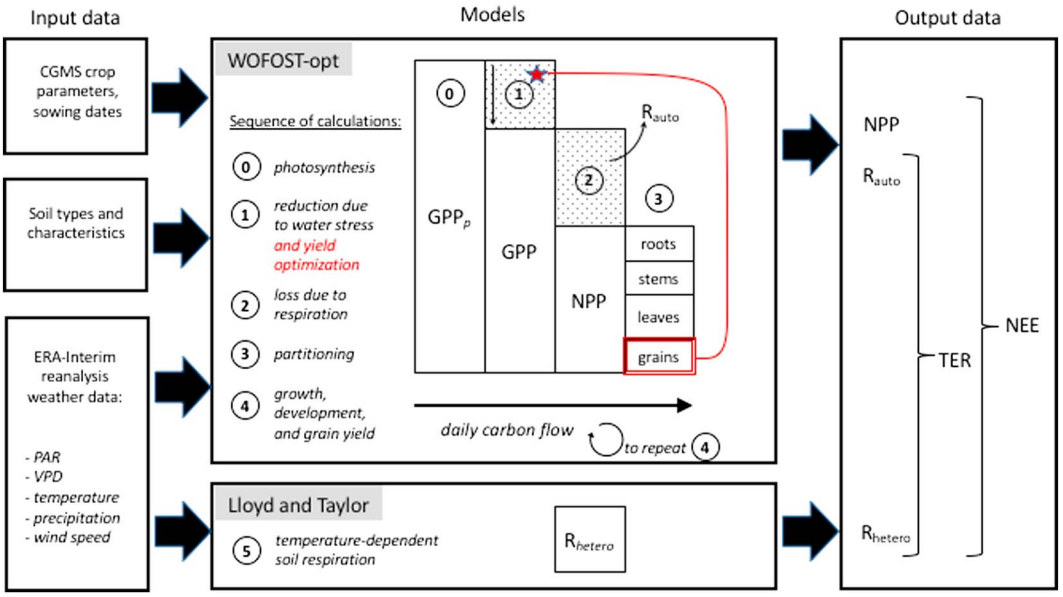

Figure 1. Flowchart of the modeling framework used in this study. We see that only few crop processes are explicitly represented (i.e., have their own equation) in the WOFOST model. These are the basic crop growth processes (i.e., photosynthesis, respiration, dry matter partitioning, and development) and one crop growth-limiting factor (water stress). The purpose of the added optimization described in section 3.2 is to take into account all other nonrepresented growth-limiting processes (e.g., nutrient stress, pests, diseases, animals, and other disturbances) to downscale GPP according to reported observations of grain yields (see equation (4)). Finally, we see here that we complete the optimized WOFOST model (WOFOST-opt) with a model for heterotrophic respiration in order to obtain the net cropland ecosystem exchange (NEE).

The autotrophic respiration (R_{aut}, in $g_C\ m^{-2}\ d^{-1}$) is then computed (see equation (7)) and added to GPP. R_{aut} is composed of two types of respiration. First, maintenance respiration (R_{maint}) represents the energy cost of maintaining the plant cell structural material. Second, growth respiration (R_{grow}) is the energy cost to transform any leftover assimilates into structural plant cell material. The following expressions are used to parameterize both processes:

$$R_{maint} = R_{m,25} \times Q_{10}{}^{(Tair-25)/10}, \tag{5}$$

$$R_{grow} = (-\mathrm{GPP} + R_{maint}) \times (1 - r_{conv}), \tag{6}$$

$$R_{aut} = R_{maint} + R_{grow}, \tag{7}$$

with $R_{m,25}$ the reference maintenance respiration rate at 25°C in $g_C\ m^{-2}\ d^{-1}$, related to the size of plant carbon pools to maintain and their age, Q_{10} the relative increase in R_{maint} with each 10°C increase, T_{air} the daily mean air temperature in °C, and r_{conv} the species-dependent conversion efficiency of carbon into dry matter.

The assimilated matter that has not been respired (−GPP-R_{aut}) is then allocated to the different plant organs: the leaves, stems, roots, and grains/tubers (see Figure 1). The matter that is ultimately stored in the grain pool at crop maturity constitutes the so-called "grain yield" or "yield" (GY, in $kg_C\ ha^{-1}$):

$$\mathrm{GY} = \sum_{t=\mathrm{doe}}^{\mathrm{dom}} \left(\text{-GPP(t)} - R_{aut}(t)\right) \times A_g(\mathrm{DVS}(t)), \tag{8}$$

with doe and dom, respectively, the day of emergence and day of maturity, and A_g the allocation factor to the grain pool, which itself is a function of the crop developmental stage (DVS(t)). Note that GY is the variable that we compare to observations for the model optimization (see section 3.2).

Finally, note that carbon exchange and storage in the plant organs is computed per m^2 of ground area, which means that WOFOST is not spatially explicit. We use soil, crop, and weather information at a 25 km resolution (see section 3.1) to enable the spatial representation of crop GPP and R_{aut}.

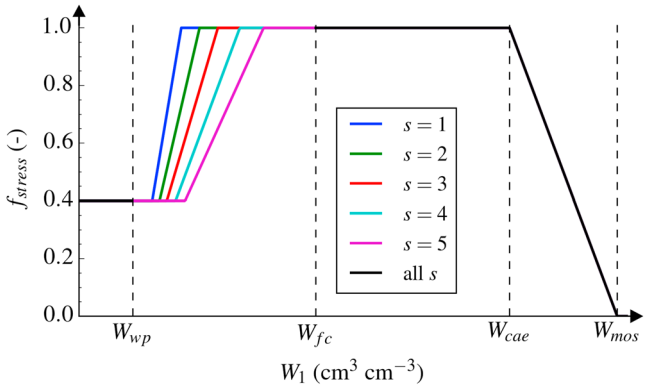

Figure 2. Water-stress downscaling factor of daily GPP and transpiration. Key soil moisture contents are indicated with dashed lines: W_{wp} is the wilting point, W_{fc} the field capacity, W_{cae} the critical point for aeration, and W_{mos} the maximum oxygen stress point. In WOFOST-WLP, crops are categorized in groups from drought sensitive ($s = 5$) to drought resistant ($s = 1$). Potatoes, sunflower, peas, and beans are listed in crop group 3, cereals in group 4 or 5, and maize in group 5. Above field capacity, all drought sensitivity groups assume the same water-excess stress response.

2.2. Crop Water-Stress Responses

WOFOST-WLP is coupled to a simple soil moisture model to evaluate the effect of water stress on crop growth (see f_{stress} in equation (4)). Two soil layers are defined: (1) the upper "rooted" soil layer and (2) the lower explorable soil layer expanding down to the maximum rooting depth (a soil- and crop-dependent parameter). Note that the depth of the rooted layer (RD, in cm) increases along time as the crop roots accumulate carbon and expand downward. To compute the daily crop water stress, we evaluate the daily water balance of the upper soil layer. The volumetric soil moisture content of that upper layer (W_1, in cm^3 cm^{-3}) is the result of the previous day's content ($W_{1,i}$), and of the modeled daily incoming and outgoing water fluxes (all in cm d^{-1}): precipitation (P), evapotranspiration (ET), free drainage (D), and runoff (R):

$$W_1 = W_{1,i} + \frac{P - ET - D - R}{\mathrm{RD}}\Delta t, \tag{9}$$

with Δt the time step of 1 day. We assume in this water flow scheme no irrigation, no capillary rise from the groundwater, and no exchange of water between grid cells (i.e., no routing). For every individual crop growth run, we initialize soil moisture to be at field capacity at sowing date before allowing it to vary in time with the local incoming and outgoing fluxes of water. Every day, the amount of soil moisture W_1 is used to estimate a dimensionless water-stress factor f_{stress} — shown in Figure 2 — that directly downregulates daily GPP and R_{growth}. Under water-limited conditions (i.e., below field capacity), the type of water-stress response function is dependent on the plant species, until we reach the lower threshold of 0.4 for f_{stress}. This lower threshold ensures that we represent the effect of irrigation on crop growth during severe droughts, as we assume here that farmers irrigate to prevent crop failure. We discuss this simple representation of irrigation in the discussion section.

2.3. Soil Respiration and Net Ecosystem Exchange

To complete the CO_2 exchange budget at the surface, we use the Lloyd and Taylor (1994) model to compute the instantaneous soil respiration ($R_s(t)$, in mg$_{CO_2}$ m^{-2} s^{-1}), and which represents a sigmoidal increase in soil respiration with soil temperature:

$$R_s(t) = R_{10} \times \exp\left(\frac{E_a}{283.15\ R^*} \times \left(1 - \frac{283.15}{T_s(t)}\right)\right), \tag{10}$$

with R_{10} the base respiration rate at 10°C, E_a the ecosystem sensitivity coefficient in K, R^* the universal gas constant, and $T_s(t)$ the instantaneous upper soil layer temperature in K. This Lloyd and Taylor (1994) model reportedly performs better than Q_{10} exponential models over wide ranges of temperature. To parameterize the site parameters R_{10} and E_a and since we do not have values readily available for croplands, we use an R_{10} of 0.08 mg$_{CO_2}$ m^{-2} s^{-1} and an E_a of 53 kJ kmol^{-1}, two reasonable values measured at grassland sites in the Netherlands (Jacobs et al., 2007). Also, since we do not have soil temperature in the reanalysis weather data, we replace T_s in equation (10) with the 2 m air temperature (T_{air}), assuming that the error introduced by the larger diurnal amplitude of T_{air} will average out over 24 h. We hence compute the daily soil respiration (R_{soil}, in g$_C$ m^{-2} d^{-1}) by integrating R_s over a day and converting it from mg$_{CO_2}$ to g$_C$ with a conversion factor (C_f):

$$R_{soil} = C_f \times R_{10} \int_{t=00:00\ \mathrm{LT}}^{t=23:59\ \mathrm{LT}} \left\{\exp\left(\frac{E_a}{283.15\ R^*} \times \left[1 - \frac{283.15}{T_{air}(t)}\right]\right)\right\} \mathrm{d}t. \tag{11}$$

We have evaluated that the larger diurnal amplitude of T_{air} introduces an overestimation of R_{soil} of on average +10% (not shown here).

The total exchange of CO_2 at the surface (or net ecosystem exchange — NEE — in g$_C$ m^{-2} d^{-1}) is finally the result of all daily fluxes of photosynthesis and respiration:

$$\begin{aligned} \mathrm{NEE} &= \mathrm{GPP} + \mathrm{TER}, \\ &= \mathrm{GPP} + R_{grow} + R_{maint} + R_{het}, \end{aligned} \tag{12}$$

with TER the total ecosystem respiration and R_{het} the heterotrophic respiration generated by soil microbial activity. Note that in practice, the R_{10} and E_a parameters from equation (10) were estimated from nighttime eddy-covariance NEE measurements, when no GPP and no R_{growth} occur (see Jacobs et al., 2007). As a result, R_{soil} represent not only R_{het} as originally intended but also the whole plant maintenance respiration, both variables dependent on T_{air}. Since we cannot extract R_{het} from the soil respiration model and to avoid double counting R_{maint}, in this study we compute NEE by adding R_{soil} to the GPP and R_{grow} from the WOFOST-WLP model:

$$\mathrm{NEE} = \mathrm{GPP} + R_{grow} + R_{soil}. \tag{13}$$

3. Material and Methods

3.1. Model Input Data and Spatial Implementation

To model crop growth, we provide three types of input data to the WOFOST-WLP model: crop parameters, soil parameters, and weather data. As mentioned earlier, WOFOST-WLP is not spatially explicit as it represents crop growth per m^2 of ground area. This means that the spatial resolution and domain of the model are set entirely by the input data itself. In our study, we provide the WOFOST-WLP model with spatially varying crop and soil parameters taken from the Crop Growth Monitoring System (CGMS, see Boogaard et al., 2013). The CGMS database contains crop calendars and variety parameters for the 10 most grown crop species in Europe (wheat, barley, grain and fodder maize, sugar beet, potato, rye, rapeseed, sunflower, and field beans) on a 25×25 km grid (see a summary of key crop parameters in Table A1, in Appendix). These parameters have been established on an ensemble of crop trials conducted in Europe. The CGMS database also contains soil types information on an even finer 1:1 000 000 scale, and thus, several soil types are listed in each 25×25 km grid cell. The CGMS database for crop and soil parameters currently covers a large European domain, extended to Russia up to the Ural Mountains, to Anatolia, and to the Maghreb. For this study, we focus on regions for which both CGMS data and EUROSTAT crop yield observations are available (see section 3.2). This covers the 28 European Union (EU) member states, the EU candidate countries (Montenegro, Macedonia, Albania, Serbia, Kosovo, Bosnia-Herzegovina, and Turkey), and the European Free-Trade Association countries (Iceland, Norway, Liechtenstein, and Switzerland). For a few extra countries (Belarus, Ukraine, Russia, Georgia, Armenia, and Azerbaijan), we also provide calculated fluxes where we have CGMS input data but these are not based on optimized yield-gap factors in the absence of reported yields to EUROSTAT. Possibly, other data sources (such as from the United Nations Food and Agricultural Administration, or the Food and Agriculture Organization of the United Nations) can be explored in the future to expand our optimization domain.

In addition to initializing the model with crop and soil parameters from the CGMS database, we provide it with weather driver data. We use the 3-hourly $1° \times 1°$ ERA-Interim reanalysis weather data from the European Centre for Medium-Range Weather Forecasts (ECMWF) model (Dee et al., 2011), which we transfer onto the finer CGMS grid without downscaling. With this combination of data, we assume homogeneity of crop parameters and weather conditions over one 25×25 km CGMS grid cell, but heterogeneity of soils below our 25 km resolution, as several soil types are available per grid cell.

3.2. Crop Growth Optimization

The WOFOST-WLP model represents the crop potential growth in a given weather and soil environment, and its possible reduction by water stress. The model thus neglects the impact of additional growth-limiting factors such as nutrients, weed, pests, diseases, and other disturbances. To bridge the gap between the modeled and the actual levels of crop production, we integrate grain yield observations to optimize a crop growth scaling factor, the yield gap factor (f_{gap}). This factor directly multiplies the daily GPP computed by the WOFOST-WLP model (see equation (4)) and thus generates a nonlinear reduction of the final crop standing biomass. Due to the spatial and temporal coverage of the observations we use in our optimization procedure, we compute one optimum f_{gap} per year, crop, and observed region, as described below.

3.2.1. Observations Used for Optimization

In this study, we use the observed yields from the Statistical Office of the European Union (EUROSTAT, 2015). The EUROSTAT yields of all major European crop species are reported by the EU member and candidate member states at four administrative regional levels, the so-called NUTS 0 (national) and NUTS 1, 2, and 3 (subnational) levels. Reports of grain yields are only compulsory at the NUTS 0 level. We use the NUTS 2 records in order to obtain a higher spatial resolution on the optimized crop growth where observations are available. Otherwise, in NUTS 2 regions and years where observed records are missing, we use instead the upper NUTS

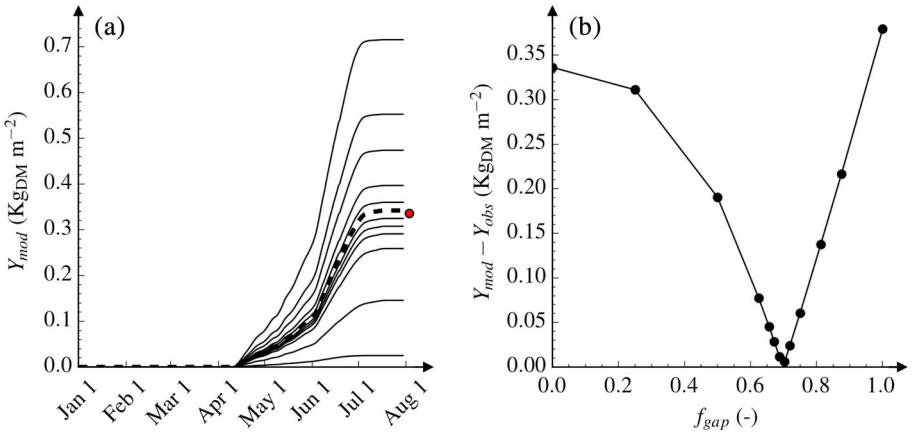

Figure 3. Example optimization of the winter wheat growth in Spain, 2013. (a) The evolution along time of Y_{mod} for the 13 tested values of f_{gap}. (b) The absolute $Y_{mod} - Y_{obs}$ difference for these 13 runs. We find the optimum run (thick dashed line in Figure 3a) is the one that reaches the observed yield (red circle) best, resulting in the lowest $Y_{mod} - Y_{obs}$ residual in Figure 3b.

level records (NUTS 1 or if fails, NUTS 0) to estimate the optimum f_{gap}. In the absence of observations, we use either the yield-gap factor from an adjacent year, from a multiyear average, or a standard value of 0.66. The latter represents a typical value found across Europe in our optimizations.

3.2.2. Optimization Procedure

Because the EUROSTAT observations are reported on a larger scale than the model grid scale, the first step of the optimization is to aggregate the gridded yields to the same spatial resolution as the observations. For that, we execute an ensemble of 30 runs per NUTS region with the WOFOST-WLP model, for a given crop and year. This ensemble is created by selecting the top 10 grid cells containing the largest fraction of arable land in a NUTS region, and the top 3 soil types that are most present within these grid cells. The modeled regional yield is then approximated by a weighted average of the 30 yields, using soil type areas as weighing factors:

$$Y_{\mathrm{mod}} = \frac{\sum_{i=1}^{10}\sum_{j=1}^{3}\left(a_{i,j} \times \mathrm{GY}_{i,j}\right)}{\sum_{i=1}^{10}\sum_{j=1}^{3} a_{i,j}}, \tag{14}$$

with Y_{mod} the aggregated modeled yield, i the gril cell number, j the soil type number, $\mathrm{GY}_{i,j}$ a single-run grain yield from the 30-run ensemble, and $a_{i,j}$ the soil type area of the same run. The difference between Y_{mod} and the reported regional yield (Y_{obs}) is then computed to determine the optimum f_{gap}. We iteratively explore 13 values of f_{gap} between 0 and 1, every time dividing its exploration range by two, and retain the optimum as the value that minimizes the absolute $Y_{\mathrm{mod}} - Y_{\mathrm{obs}}$ difference (see Figure 3). Note that the optimum f_{gap} cannot be greater than 1. Our assumption is then that by optimizing crop yield, we bring crop growth and crop CO_2 exchange down to their actual levels over diurnal and seasonal time scales. We repeat that f_{gap} is directly coupled to plant development and evapotranspiration and therefore influences the value of f_{stress}, which makes our method nonlinear especially toward the regimes where water limitations play an important role. We evaluate our framework by comparing the modeled crop CO_2 fluxes against independent observations.

3.3. Model Validation

3.3.1. Independent CO_2 Flux Observations

We validate the fluxes of GPP, TER, and NEE generated by the optimized WOFOST-WLP model (hereafter referred to as WOFOST-opt) with independent observations at seven FluxNet sites. These sites are located within three important climate zones of Europe: a Mediterranean (Csa), a temperate (Cfb), and a cold zone (Dfb, see Table 1), and they were cultivated with eight different crops (out of the 10 species we simulate over Europe) during various periods between 2000 and 2014 to make a total of 40 site years of validation data. All sites measured NEE on a half-hourly basis using the eddy-covariance technique and following the FluxNet protocol. Measurements of NEE were filtered for low friction velocities using an interannually variable

Table 1
List of Selected FluxNet Sites

Site ID	Country	Longitude	Latitude	Climate	NUTS 2 region	CGMS grid cell ID	Reference papers
BE-Lon	Belgium	4.74	50.55	Cfb	BE35	100094	Moureaux et al. (2006)
DE-Kli	Germany	13.52	50.89	Cfb	DED2	102119	Prescher et al. (2010)
FI-Jok	Finland	23.51	60.90	Dfb	FI1C	148139	Lohila et al. (2004)
FR-Gri	France	1.95	48.84	Cfb	FR10	94086	Loubet et al. (2011)
IT-BCi	Italy	14.96	40.52	Csa	ITF3	56126	Vitale et al. (2007)
NL-Dij	Netherlands	5.65	51.99	Cfb	NL31	107097	Jans et al. (2010)
NL-Lan	Netherlands	4.90	51.95	Cfb	NL33	106095	Moors et al. (2010)

Note. Climates were classified using the Köppen-Geiger classification from Peel et al. (2007).

threshold, then gap-filled and partitioned into TER and GPP using the nighttime method of Reichstein et al. (2005). More information about the crop rotation and management of the different sites can be found in Table B1. All sites have been fully described in previous publications (see the reference papers cited in Table 1).

3.3.2. The SiBCASA Terrestrial Biosphere Model

We use the SiBCASA model (Schaefer et al., 2008; van der Velde, 2015) to compare our results to a terrestrial biosphere model. SiBCASA is a typical example of a TBM that uses the concept of plant functional types. It has been widely used in studies of atmospheric CO_2 (Alden et al., 2016; Peters et al., 2010), CO_2 isotopes (van der Velde et al., 2014), and carbon-climate interactions (Hope & Schaefer, 2015; Richardson et al., 2011; van der Molen et al., 2016). For our study, we compute fluxes of GPP, TER, and NEE for the seven grid cells where the FluxNet sites are located, using the cropland PFT parameters. We drive SiBCASA with $1^\circ \times 1^\circ$ soil moisture and meteorological data from the same ERA-Interim reanalysis as in section 3.1 (Dee et al., 2011). We start all our runs from steady state, which is obtained with an analytic spin-up of the model (i.e., we iteratively run SiBCASA with the same 10 year meteorological forcing data, until we meet our steady state criteria). We consider that steady state is reached when the yearly average NEE flux equals less than 1% of the yearly average GPP flux, hence generating stable soil carbon pools over time.

4. Results

4.1. Crop Growth Optimization

The optimization of the crop growth scaling factor (f_{gap}) in WOFOST-opt allows us to reproduce the interannual variability of regionally observed grain yields from EUROSTAT. As an example of a region with a large yield gap, the upper time series in Figure 4a presents the modeled grain yields before and after optimization of f_{gap} for spring barley over the NUTS regions of Castilla y León in Spain. After optimization in Figure 4a, the remaining difference between optimized and observed yields is only about 2% on average over the years 2000–2014. On a few occasions, the optimization corrects year-to-year variations of grain yield (e.g., the yield variation from 2002 to 2003 is changed from decreasing to increasing). The long-term upward trend in the observed grain yields (i.e., the linear yield increase of $+11.33 \times 10^{-4}$ kg_{DM} m^{-2} yr^{-1} from 2000 to 2014) is also captured after the optimization. This trend, referred to as the technology trend by de Wit et al. (2010), can be explained by the ongoing improvements in farming techniques, grain quality, and industrial crop management. Note that low yields in the time series indicate agricultural drought years in this region of Spain, like for 2005 (confirmed in Spinoni et al., 2015), and we study this example in more detail in section 4.4.

In addition to year-to-year changes, our optimization captures substantial spatial variability of observed grain yields and yield gap factors. Figure 4b shows the optimum f_{gap} over Europe for winter wheat in 2013, the crop with the best yield data coverage at the NUTS 2 level in EUROSTAT. After optimization, the highest modeled yields and f_{gap} are in Western Europe, and the lowest are in Scandinavia and Southern Europe, which is a typical spatial pattern for wheat and barley (see also Bondeau et al., 2007). The optimum f_{gap} varies from 0.48 to 1.0 across Europe, which implies that simply using an average value of f_{gap} across the continent would have resulted in significant spatial errors on the optimized yields. With the spatiotemporal variability driven by the EUROSTAT yield records, we expect our WOFOST-opt model to have well-constrained crop carbon

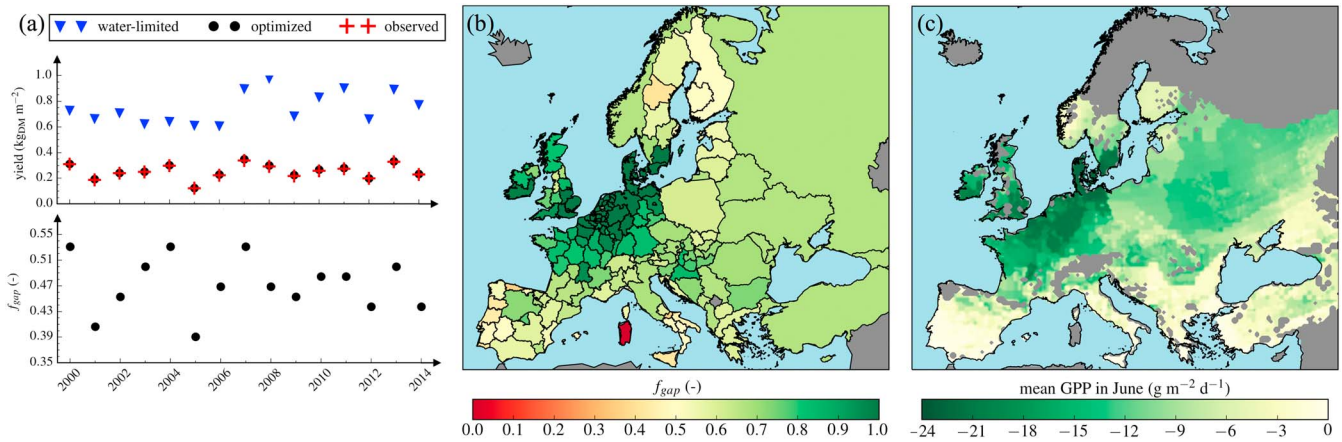

Figure 4. Variability of the assimilated observations and resulting model optimization. (a) The temporal variability of the modeled (water limited and optimized) and observed grain yields for the example of spring barley in the Spanish NUTS 2 region Castilla y León (in the top panel), and the corresponding optimum f_{gap} values of each year (in the bottom panel). Note that the optimum f_{gap} can range from 0 to 1 and directly multiplies daily GPP throughout the season, as shown in equation (4). (b) The spatial variability of the optimum yield gap factor computed for winter wheat in 2013, resulting in the (c) optimized GPP.

accumulation locally, and a more reliable representation of cropland GPP, TER, and NEE over the growing season. To validate this, we analyze next the modeled crop CO_2 fluxes that lead to these optimized grain yields.

4.2. Daily CO_2 Exchange

We find that the WOFOST-opt model represents the crop-specific growing season length (a short 2–3 months period) and magnitude of the productivity (from 10 to 30 $g_C\ m^{-2}\ d^{-1}$) very well. This is shown in Figures 5a–5f for a subset of the available years and sites from the FluxNet database. Across three very different climate zones of Europe, and for six of the most grown crops in Europe (winter wheat, grain maize, spring barley, potato, sugar beet, and winter rapeseed), we see the correspondence of GPP and TER to daily observations is satisfactory, and also clearly much better than the SiBCASA model estimates at these locations. This improvement is most evident in the phenology as WOFOST-opt matches the local growing season length, except for an overestimation at all potato sites (e.g., 6 weeks in Figure 5a). WOFOST-opt also captures the strong interspecies differences in terms of maximum GPP much better (e.g., highest is 20–30 $g_C\ m^{-2}\ d^{-1}$ for maize, lowest is 8–10 $g_C\ m^{-2}\ d^{-1}$ for barley). An exception is seen for the Italian site where we find an overestimation of GPP by WOFOST-opt (cf. Figure 5f), which is further discussed in section 4.4.

The improved phenology and seasonal cycle amplitude of Figure 5 translates into much higher values of the coefficient of determination (R^2) of NEE for WOFOST-opt when compared to SiBCASA across all sites of Table 2, except in the Mediterranean one (i.e., the IT-BCi site). However, these high R^2 scores do not necessarily translate into lower RMSE values (only for 10 out of 17 crop sites), partly because time shifts of the seasonal cycle carry a high penalty in RMSE (e.g., BE-Lon in Figure 5c). Note that these time shifts occur because we did not use local sowing dates to set up our framework here, and most sites RMSE decrease substantially if we do use them (not shown here). For our Mediterranean site, we obtain a poor R^2 and RMSE mostly because our framework does not take into account local irrigation practices, and our modeled water stress strongly modifies the shape of the seasonal cycle (see Figure 5f; also, see further analysis in section 4.4). The overall good seasonality and high R^2 values of WOFOST-opt in the cold and temperate climate zones nevertheless demonstrate that our modeling framework can generate good estimates of the daily cropland CO_2 exchange at a large number of sites across Europe. Our novel application of grain yield data thus puts new constraints on the CO_2 exchange of European croplands. To complete and extend our evaluation, we analyze the interannual variability of the cropland CO_2 exchange for a well-watered location in Belgium. Further analysis of the cropland CO_2 exchange during droughts in the Mediterranean region then follows in section 4.4.

4.3. Decadal CO_2 Exchange

The WOFOST-opt model optimized with EUROSTAT grain yield data is able to represent the interannual variability of crop CO_2 exchange that is driven by the crop rotation on a field. This is because the crop model accounts for interspecies differences in phenology and photosynthetic rates. Figure 6 compares the WOFOST-opt GPP, TER, and NEE fluxes against 10 years of observations at the BE-Lon FluxNet site in Belgium.

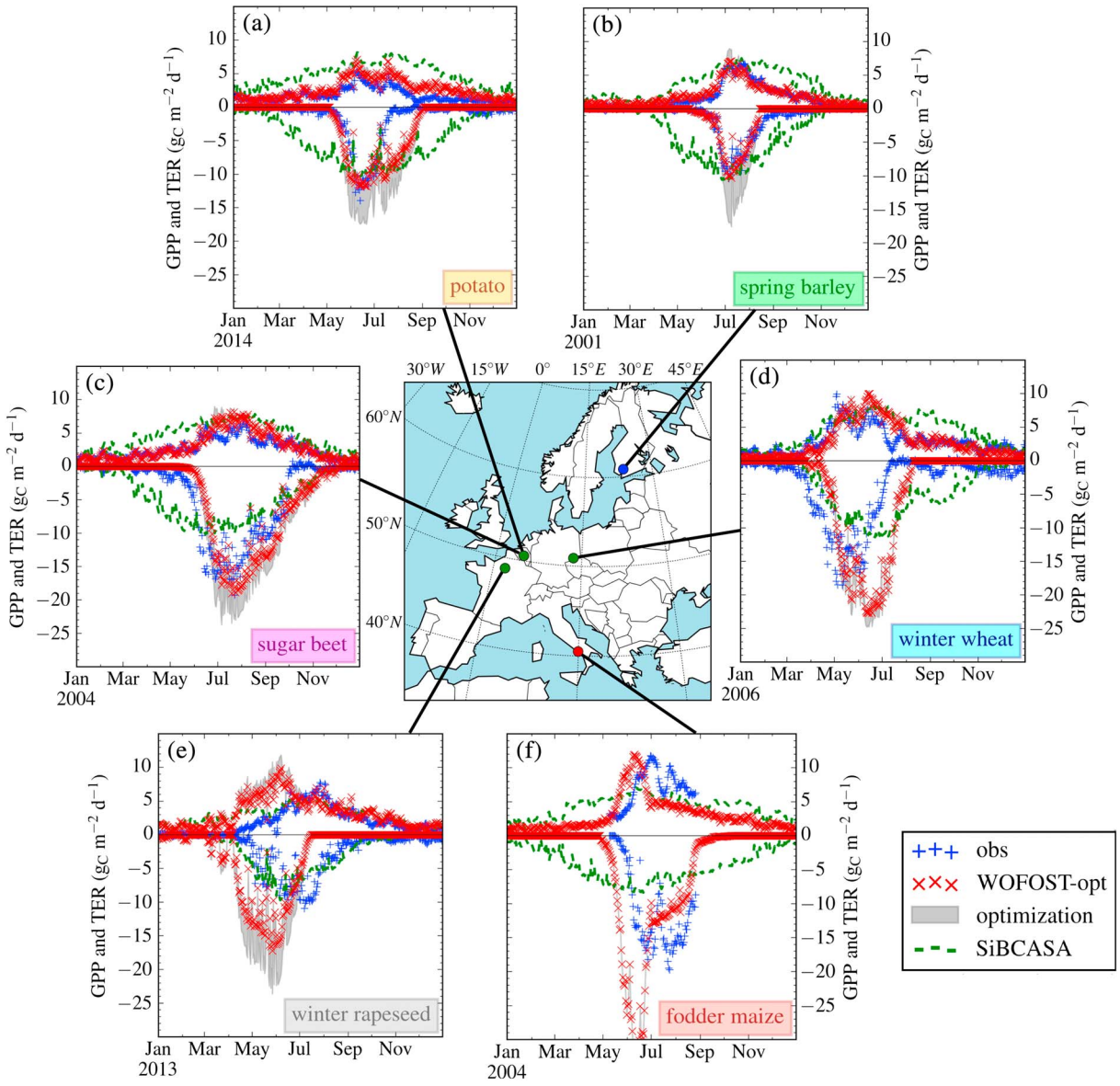

Figure 5. (a–f) Comparison of WOFOST-opt against local observations of daily GPP (negative values) and TER (positive values). Note that the WOFOST-opt runs are not adapted to fit the local growth conditions as they use CGMS sowing dates and EUROSTAT yields. We present here a subset of all 40 sites and years available (see selection in Table B1), covering three major European climate zones: Mediterranean (red dot on the map), temperate (green dots), and cold (blue dot). We specifically represent the improvement made when switching from the nonoptimized to the optimized WOFOST model with the grey areas. Thus, when the computed f_{gap} is equal to 1, there is no such improvement (e.g., Figure 5f). We also plot the SiBCASA cropland-PFT fluxes for the same site and years. We see the WOFOST model has a much better crop phenology than SiBCASA.

This site conserves a sugar beet/winter wheat/potato/winter wheat crop rotation from 2004 to 2014, with one exception of a grain maize year. Over this decade, we computed an optimum f_{gap} that ranges from 0.69 (in 2014) to 1.0 (in 2006 and 2010), using EUROSTAT crop yields. WOFOST-opt captures the timing of local growing season and the amplitude of the GPP and TER fluxes well every year from crop to crop at site BE-Lon, although differences of up to one third of the observed maximum fluxes can be observed. Note that shifts in the growing season not exceeding 2 weeks for this particular site can occur, the largest shift occurring in early spring 2007. Twice in this decade (in 2009 and 2013), mustard was planted after the harvest of winter wheat, just before the following winter period (see Kutsch et al., 2010). This is a local feature in the observations that cannot be captured by our crop model, as it only represents the growth of one crop sown on site. Despite this, the overall agreement of the regionally optimized WOFOST-opt is very good at the Belgian site, with a 10 year

Table 2
Statistics of Three NEE Models: (a) SiBCASA (SIB), (b) the Nonoptimized WOFOST (WOF), and (c) the Optimized WOFOST (OPT) Over 40 Years of FluxNet Measurements (see Tables 1 and B1)

	Number of years	Climates	RMSE on NEE (g_C m^{-2} d^{-1}) SIB	WOF	OPT	R^2 of NEE model (-) SIB	WOF	OPT	Min-Max optimum f_{gap} range
Winter wheat									0.67-1.00
FR-Gri	3	Cfb	3.27	3.28	2.67	0.28	0.69	0.70	
DE-Kli	2	Cfb	2.23	3.13	2.46	0.57	0.77	0.64	
BE-Lon	5	Cfb	3.70	2.91	2.33	0.39	0.78	0.74	
Grain maize									0.70-1.00
FR-Gri	2	Cfb	3.21	4.45	4.32	0.37	0.59	0.52	
BE-Lon	1	Cfb	3.48	4.53	2.25	0.23	0.78	0.68	
NL-Lan	1	Cfb	2.83	6.10	4.51	0.17	0.42	0.46	
Fodder Maize									0.88-1.00
IT-BCi	6	Cfa	5.99	8.66	7.21	0.15	0.00	0.05	
FR-Gri	1	Cfb	4.05	4.34	4.18	0.51	0.54	0.57	
DE-Kli	2	Cfb	2.64	6.11	5.56	0.05	0.53	0.62	
NL-Dij	1	Cfb	5.12	5.05	4.29	0.14	0.78	0.82	
Winter barley									0.67-0.80
FR-Gri	2	Cfb	3.52	2.34	2.32	0.14	0.85	0.88	
DE-Kli	3	Cfb	3.71	3.28	2.11	0.12	0.72	0.77	
Spring barley									0.70-0.75
DE-Kli	2	Cfb	1.71	3.17	1.75	0.33	0.74	0.71	
FI-Jok	1	Dfb	1.82	1.66	0.80	0.17	0.69	0.74	
Winter rapeseed									0.83-0.94
FR-Gri	1	Cfb	2.52	2.44	1.86	0.39	0.86	0.85	
DE-Kli	2	Cfb	2.67	3.14	2.64	0.25	0.71	0.70	
Potato									0.69-1.00
BE-Lon	3	Cfb	2.11	2.86	2.26	0.28	0.39	0.43	
Sugar beet									0.84-0.86
BE-Lon	2	Cfb	4.59	2.71	1.69	0.29	0.77	0.88	

RMSE of 2.58 g_C m^{-2} d^{-1} for GPP and 1.21 g_C m^{-2} d^{-1} for TER, not exceeding 10% of the max-min range of the observed respective variables, and an R^2 of 0.80 and 0.71 for GPP and TER over the decade. This translates into a NEE with a correct interannual pattern ($R^2 = 0.67$) as can be seen in Figure 6. Finally, and to place our findings in a broader context, we note that this interannual variability is typically not included at all in the SiBCASA TBM (see Figure 6), as it uses the same cropland constants every year. We infer that our WOFOST-opt model is better suited than a TBM like SiBCASA to represent the temporal variations of cropland CO_2 exchange, from the diurnal to the seasonal and decadal scales. While this is true at most locations, we find the performance of WOFOST-opt drops under extreme water stress (e.g. in Italy, see Figure 5f), which we assess next.

4.4. Cropland CO_2 Exchange During Droughts

We show in section 4.2 that our modeling framework is sometimes not able to optimize crop growth during drought stress, like for the Italian site of Figure 5f and Table 2. Here we further examine the behavior of our framework during a reported drought year (i.e., the severe drought of 2005 that occurred over the Iberian peninsula, see Figure 4a), as it links closely to the poorer representation of the Italian site. The Iberian 2005 drought was characterized by a large precipitation deficit from October 2004 to June 2005, especially severe in the southern half of the peninsula (up to −60% of the normal cumulated precipitation, see García-Herrera et al., 2007). That deficit resulted in a large decrease in crop production, especially for barley and wheat

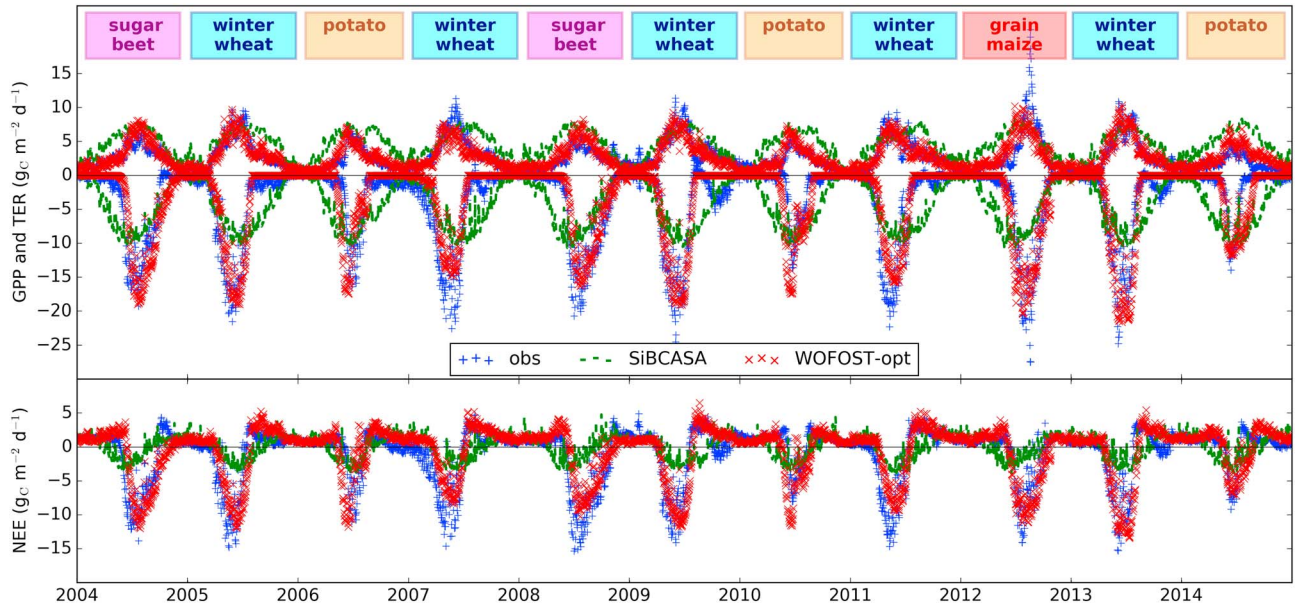

Figure 6. Ten years of observed and modeled GPP, TER, and NEE fluxes at the Belgian FluxNet site BE-Lon. Note that the WOFOST-opt runs are not adapted to fit the local growth conditions as they use CGMS sowing dates and EUROSTAT yields.

(up to −60% of the 2004 yield, see European Commission, 2005; García-Herrera et al., 2007; and Gouveia et al., 2009), which occupy together about a third of the total arable land area of the peninsula (EUROSTAT, 2015). We now model this major agricultural drought event with our WOFOST-opt framework.

For this, we optimize crop growth for the top eight crops of Spain and Portugal and compute area-weighted carbon fluxes for years 2004 and 2005. Over the Peninsula, the average cropland fluxes are thus composed of (1) 48% spring barley, (2) 26% winter wheat, (3) 11% grain maize, (4) 8% winter barley, (5) 3% potato, (6) 3% fodder maize, (7) 2% sugar beet, and (8) less than 1% spring wheat. Figure 7 presents the cropland carbon flux anomalies for 2005 as calculated by our WOFOST-opt framework. We compare our results to those of the cropland PFT of the SiBCASA model, produced with the same meteorological forcing data.

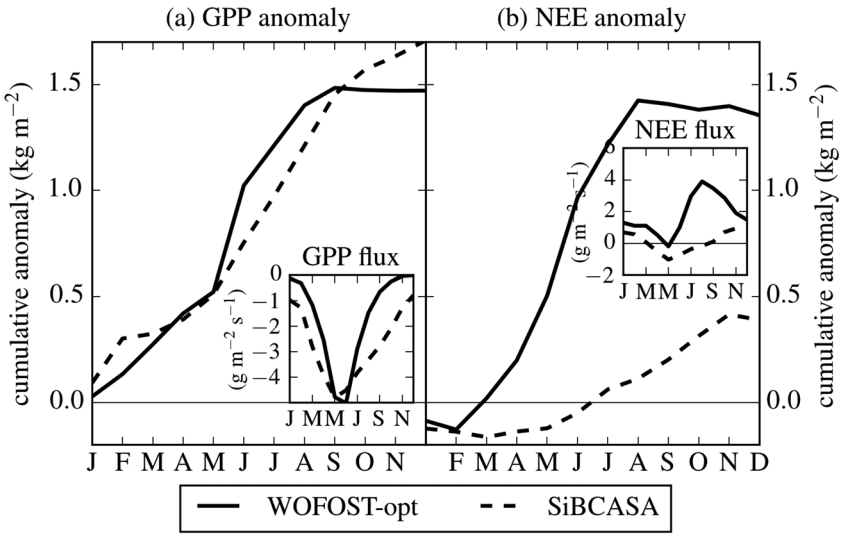

Figure 7. The Iberian 2005 drought as seen by WOFOST-opt and the SiBCASA cropland PFT. Throughout Figure 7, the 2005 anomaly represents year 2005 as compared to 2004 by the same model. As a result of their methodological differences (especially phenology and respiration), WOFOST-opt and SiBCASA compute very contrasting NEE flux anomalies during this 2005 drought.

The timing of the drought impact on the crop carbon exchange is quite different between the two models, mainly due to their difference in crop phenology. Figure 7 show that the accumulation of carbon flux anomalies (both GPP and NEE) stops around August–September 2005 for WOFOST, toward the end of its growing season (see the GPP flux in the inset of Figure 7a). SiBCASA on the other hand unrealistically continues its cropland carbon exchange until December, which causes it to detect flux anomalies much later in the year. Overall, both models accumulate a similar total GPP anomaly by the end of the growing season (1.5 kg m^{-2} in August 2005, see Figure 7b). Nevertheless, the model differences in phenology imply that this cumulated GPP anomaly represents only 11% of the yearly total GPP for SiBCASA, while it represents 17% of the yearly GPP of WOFOST-opt. Our findings imply that the impacts of the 2005 drought on crop growth was seen as more severe by WOFOST-opt than by SiBCASA, in line with the reported extreme agricultural impacts over the Peninsula (e.g., in Portugal, see Gouveia et al., 2009). The strength of the drought signal is constrained by the crop yield reduction during the optimization of WOFOST, which is a strong point of our method. The better phenology of the WOFOST model finally ensures that carbon flux anomalies occur during the actual crop growing season (i.e., before the summer in the Iberian peninsula).

The absence of water-stress effects on soil respiration in WOFOST-opt is a current limitation of the model, which causes the TER and NEE drought anomalies to be very different between the two models. Indeed, as we can see in equation (10), heterotrophic respiration is a function of soil temperature only. This causes the TER flux to be generally larger than the one of GPP throughout 2005 in WOFOST-opt, especially in summer when the crop growth has stopped but high temperatures still generate high respiration fluxes. As a result, the NEE flux of WOFOST-opt (see inset of Figure 7b) is always positive during the 2005 drought. On the other hand, the SiBCASA model expresses heterotrophic respiration as a function of both soil temperature and soil moisture, which causes its TER to be much smaller than in WOFOST-opt in 2005 due to the drought, and which causes its yearly average NEE to be close to zero. The differences in the implementation of TER between the models thus generate very contrasting negative TER anomalies (−1.3 and −0.2 kg m^{-2} for, respectively, SiBCASA and WOFOST-opt by the end of August), producing the much higher positive NEE anomaly for WOFOST in Figure 7b. This positive anomaly (which means that the peninsula is seen as a net source of CO_2 by the model) is most probably unrealistic as studies have shown the dependence of soil respiration on soil moisture stress, especially in semiarid regions like the Mediterranean (e.g., Carbone et al., 2011; Conant et al., 2004; Moyano et al., 2013). Our 2005 Iberian drought case thus puts forward the necessity to implement a water-stress limitation on soil respiration. Such implementation is planned in the near future for WOFOST-opt.

Finally, it is important to realize the impact of irrigation in drought events. The 2005 drought in the Iberian peninsula was so severe that the lower threshold of water stress (i.e., $f_{stress} = 0.4$) set in our model was reached in 21% of the grid cells of the peninsula (mostly in the Spanish region of Extremadura and on the southeast coastline). Without this simple constraint on f_{stress} to represent irrigation, crop failure (i.e., no grain filling) massively occurs with WOFOST-opt in these regions (not shown here). Such cases of crop failure is also what occurred in the Italian site in Figure 5f, even with our simple representation of irrigation. In practice, crop failure renders the optimization of WOFOST impossible, as the absence of a grain pool forces the optimum growth factor to be set to 1 (see optimum f_{gap} for the Italian site in Table B1). For the case of the 2005 drought in Spain and Portugal, our simplified implementation of irrigation prevented crop failure (detected as occurrences of a harvest index <5%) in all grid cells that were otherwise affected by it. This particular case of extreme drought thus brings forth the necessity of representing the impacts of irrigation on crop growth, in order to better quantify actual drought carbon exchange anomalies.

5. Discussion

5.1. Performance and Limits of the Framework

While croplands are by definition a homogeneous land surface at the crop field scale, it is not true between the crop field and our subgrid scale (i.e., 25 km scale). To account for the subgrid variability of cultivated crop species, we apply a "mosaic" approach where we compute each crop species over the spatial domain independently from each other. We then compute a cropland area-weighted average of NEE, using cultivation areas from EUROSTAT. This method is better suited to address the impact of sub-grid crop variability on the NEE fluxes than the "dominant-PFT" method (i.e., computing the fluxes from the dominant species only in each grid cell), which is for instance currently used in SiBCASA.

In our study we do not explicitly model the effects of nitrogen limitation, pests, diseases, or long-term crop breeding improvements on crop growth. These effects are likely responsible for the modeled to observed yield gaps ($Y_{obs} - Y_{mod}$). Instead, we account for these effects with the yearly optimization of the yield gap factor, following observations of crop yield. This optimization changes the overall yearly production but does not allow modifications of the seasonal crop growth pattern. We, however, do represent explicitly the effect of water stress on crop growth in the model, with a simple representation of irrigation (by applying a lower limit on the water-stress factor, see Figure 2). Our underlying assumption is that the farmers will not let their crops die due to severe water shortages, and it allows us to avoid crop failure during severe droughts (see section 4.4). However, this assumption is clearly imperfect because we do not take into account the actual availability of water, the availability of a physical infrastructure for irrigation in the region, or the economical value of the crop. The way we represent irrigation clearly matters for southern regions like the Mediterranean where irrigation is needed and frequent (Wriedt et al., 2009a). Possible misrepresentations of the seasonal cycle of NEE could thus partly be avoided by either developing irrigation rules within the model (e.g. trigger irrigation once soil moisture reaches a given threshold, as done by de Noblet-Ducoudré et al., 2004) or by supplying full irrigation information (cf. the high-resolution European irrigation map from Wriedt et al., 2009b). Moreover, with the current setup of our framework, we do not perform a continuous simulation of soil moisture. Instead, we simply initialize it to be at field capacity every year at sowing date. This "wet soil" assumption is unrealistic for the dry regions of Europe such as the Mediterranean, especially for the case of spring crops that are sown later in the year, as we could be neglecting important soil moisture depletion happening before the start of the growing season. We can solve this issue by using soil moisture data—for instance, the ERA-Interim reanalysis product (Dee et al., 2011) or perhaps remotely sensed data like in de Wit and Van Diepen (2007) or van der Molen et al. (2016)—to initialize our model.

The WOFOST model has been extensively used for research on crop yield and yield gap all over the world, notably in Europe (Bussay et al., 2015; Eitzinger et al., 2013; Foltescu, 2000; Kogan et al., 2013), Africa (Bregaglio et al., 2014; Kassie et al., 2014; Wolf et al., 2015), Middle East (Sargordi et al., 2013), India (Dua et al., 2013), and China (Wang et al., 2011). However, to our knowledge we are the first to apply WOFOST to estimate surface carbon exchange fluxes and to verify these against observations of GPP, TER, and NEE. Related to our first research question, we show the WOFOST-opt model to be a good match to the observed GPP, TER, and, NEE at the seven FluxNet sites, which we demonstrate with high R^2 values (see Table 2, but also Tables C1 and C2 in Appendix). Interestingly, for non-Mediterranean sites we find lower RMSEs are obtained for TER (with an RMSE of 1.8 $g_C\ m^{-2}\ d^{-1}$ over all 40 years of Table B1, about 8% the observed min-max range for TER) than for GPP and NEE (respectively, 5.0 and 3.9 $g_C\ m^{-2}\ d^{-1}$, about 16–17% the observed min-max range of both variables) indicating that most of the efforts to further improve NEE should be done on improving GPP at these locations. We verified that lower RMSEs can be obtained for NEE by imposing local sowing dates in the simulations of the FluxNet sites (from 3.9 to 3.2 $g_C\ m^{-2}\ d^{-1}$, or from 17% to 13% of the observed min-max range of NEE), because these effectively remove the shift in the modeled growing season as seen, for example, in Figure 5 (improvement not shown here). Our findings indicate that our framework represents a good regional estimate of cropland NEE, where water shortages are not too severe (improvements on soil respiration for heavily water-limited locations will follow in the next version of WOFOST-opt). In the end, we conclude the more realistic seasonal and interannual patterns obtained by WOFOST-opt are a clear improvement compared to the classical grassland-PFT approach of TBMs, illustrated by the example of SiBCASA.

Related to our second research question, we show that the additional integration of crop yield data into the model produces large spatial variations in the f_{gap} scaling factor, which effectively increases the spatial variability of the modeled cropland GPP and NEE toward reported levels (see European crop productivity patterns in Bondeau et al., 2007). At a number of FluxNet sites in Table 2, we observe an almost systematic improvement of the RMSE and R^2 of NEE when switching from the nonoptimized to the optimized version of the WOFOST model (except for sugar beet). However, the RMSE of WOFOST-opt is not systematically lower than the one of SiBCASA because of two factors: (a) the remaining shift in the growing season between WOFOST-opt and observations and (b) the Western Europe location of the sites, where mostly high yield gap factors occur (they are always greater than 0.7, and often close to 1, see Table 2). Larger improvements are to be expected for regions with higher $Y_{obs} - Y_{mod}$ differences, such as in Scandinavia and the Mediterranean basin (see the spatial pattern of f_{gap} in Figure 4b). While we show it is true for the Finnish site (see Table 2), we did not demonstrate

this for the Italian site since we did not take into account the irrigation practices that occurred there. As a result we obtained a substantially different seasonal cycle from reality, which was also switched earlier in time due to an earlier modeled sowing date (see Figure 5f).

Finally, and related to our third research question, we allow for the regional constraint of GPP, TER, and NEE by crop yield observations, which to a certain extent constrains the spatial variability of the carbon fluxes. By extension of Figure 4b, where we present the yield gap factor map for year 2013, we find that the winter wheat growth will be downscaled much more in the south and in Scandinavia, where the lowest grain yields are observed. This downscaling pattern is also the case for other cereal crops: maize and barley (not shown here). This explains part of the overall cropland NEE spatial variations, as most of the summer crop carbon uptake occurs over Western to Central Europe, in the midlatitudes. Moreover, and for water-stressed situations, in section 4.4 we demonstrated our framework can capture the year-to-year regional reduction in NEE caused by an agricultural drought, with some limitations on the realism of its seasonal cycle. However, improvements in the soil moisture initialization and the added representation of irrigation should remedy these limitations in water-stressed areas. Further validation of the drought response of the model could then be done by investigating the FluxNet soil moisture and evapotranspiration observations alongside the NEE measurements, where available.

5.2. Potential Applications of WOFOST-opt

Our successful validation of modeled European cropland NEE fluxes therefore opens up new possibilities for the application of WOFOST-opt in the field of carbon cycle studies, crop forecasts, land-atmosphere interactions and coupled carbon-climate experiments. First, in an uncoupled mode, WOFOST-opt can supply satisfactory past, present, and once modified as suggested in section 5.1, satisfactory future NEE boundary fluxes for atmospheric CO_2 studies. For instance, we show WOFOST-opt performs much better than SiBCASA when modeling GPP, TER, and NEE, the latter having no crop rotation and thus little interannual variability. Our model thus offers an excellent alternative for croplands in the CarbonTracker inverse modeling framework of Peters et al. (2010). The use of the WOFOST-opt model would allow us to integrate an additional stream of data (i.e., crop yields) into the atmospheric CO_2 inversions. As a fixed prior flux, it could allow to reduce the uncertainty on the posterior NEE estimates of other ecosystems, such as forest and grassland. Such analysis of the impact of WOFOST-opt fluxes is scheduled in a follow-up study.

In this study we neglected the impact of the off-site crop consumption (Chen et al., 2015). The lateral transport of crop harvest redistributes the crop products to where the population is most dense for human consumption, and to where the cattle is located for animal feed. West et al. (2011) showed a bipolar spatial pattern in the USA of production and redistribution of crop harvests, which significantly altered spatial cropland carbon fluxes. Ciais et al. (2008, 2007) also investigated the impact of crop transport and consumption over Europe, and although less clear spatial patterns emerged, they showed the release from crop consumption is similar in magnitude to the accumulation of carbon in European forests. Based on our simulated grain yield, and the aboveground biomass simulated by WOFOST-opt, our framework could be extended with a harvest module as well. In addition to the respiration or burning of crop residues, this would represent the lateral dislocation of crop harvests based on available import and export statistics across the EU.

Crop scientists have already widely explored the possibility to use WOFOST in an uncoupled crop and atmosphere setup for operational seasonal crop yield forecasts (e.g., Bussay et al., 2015; de Wit & Van Diepen, 2007), and on the longer term for crop production projections under climate change (e.g., Tao et al., 2016; Peltonen-Sainio et al., 2015). A more interesting perspective for atmospheric scientists and hydrologists though is the possibility to fully couple the WOFOST-opt model with an atmospheric model, like has been attempted by Li et al. (2013). WOFOST-opt seems to be an adequate candidate for such a coupled study because, contrarily to other models from the same line that use the evaporative demand approach (e.g., see GECROS in Combe et al., 2015), its implementation of water stress resembles the simple approach adopted by many land surface models (Camargo & Kemanian, 2016; Combe et al., 2016). Using a WOFOST-like parameterization of water stress should yield a realistic evapotranspiration and resulting energy partitioning at the surface under water-limited conditions, like has been demonstrated by Li et al. (2013). The setup would further allow users to investigate crop-atmosphere interactions, to study the interaction of crop production and drought development, and on the longer term to perform coupled carbon-climate simulations to predict crop production under future climate scenarios.

6. Conclusion

In this study, we design a crop growth modeling framework in which we assimilate European grain yield data information to constrain a model for cropland net ecosystem exchange. Our modeling framework is readily operational for the European domain, for its 10 most common crop species, at the 25 km scale. We assess its performance over Europe from 2000 to 2014, from wet to water-limited soil conditions. We find this modeling framework allows us to generate satisfactory daily to multiannual hindcasts of cropland GPP, TER, and NEE under normal to mild water-stress conditions, for a variety of crop species and climates of Europe. We quantify this improvement by computing correlation statistics on the daily CO_2 fluxes, and comparing our framework to observations performed at seven FluxNet sites. Under severe water stress like for the 2005 Iberian peninsula drought, we find the trade-off between crop growth and soil moisture depletion is largely constrained by our optimization procedure, which we show artificially modifies the shape of the seasonal cycle of NEE, although its interannual variability seems reasonable. This alteration of the seasonal cycle could be remedied by providing better estimates of soil moisture at sowing dates and by supplying irrigation information to the model. Further validation of our improved representation of soil moisture could then be done by assessing the FluxNet soil moisture and evapotranspiration measurements in combination to the NEE fluxes, at the dry cropland sites where they are both available.

Our novel framework shows promise as a new way to provide realistic cropland CO_2 fluxes to atmospheric models. The cropland fluxes computed with our optimized product will be made available to the scientific community through the ICOS Carbon Portal (http://icos-cp.eu/). In the near future, we plan to use it in a forward modeling study of atmospheric CO_2 to demonstrate the improvement it can bring on modeled atmospheric CO_2 mole fractions. We also plan to use it in an inverse modeling study of atmospheric CO_2, to assess if we can reduce the uncertainty on the European forest net carbon sink by adding a more accurate estimation of the impact of crops on atmospheric CO_2 (see van der Laan-Luijkx et al., 2017).

Appendix A: Crop Input Parameters

In this study, we have used crop and soil parameters issued from the CGMS database. This database contains ready-to-use crop and soil parameters for the WOFOST model, on a 25 × 25 km resolution (Boogaard et al., 2013). We present in Table A1 a summary of key parameter values for the geographical domain considered in section 3.1. Note that crop parameters are assumed constant from year to year but vary spatially due to variable farmer practices observed in the field.

Table A1
Crop Parameters Over Europe

Crop	Range of sowing date(s)	Range of temperature sum(s) from emergence to maturity ($°C\ d^{-1}$)	Maximum CO_2 assimilation rate ($kg_{CO2}\ ha_{leaf}^{-1}\ h^{-1}$)	Initial single leaf light-use efficiency ($kg_{CO2}\ ha^{-1}\ h^{-1}$) /($J\ m^{-2}\ s^{-1}$)	Water stress group (see Figure 2)
Winter wheat	always 1 Jan	1550 to 2670	35.83	0.45	4.5
Spring wheat	2 Feb to 18 May	755 to 2496	35.	0.4	4.5
Grain maize	24 April to 26 May	1165 to 2619	70.	0.45	4.5
Fodder maize	24 April to 26 May	1165 to 2619	70.	0.45	4.5
Winter barley	always 1 Jan	1550 to 2670	35.83	0.45	4.5
Spring barley	2 Feb to 18 May	755 to 2496	35.	0.4	4.5
Rye	always 1 Jan	1006 to 2103	35.83	0.45	4.5
Sugar beet	8 March to 4 May	1196 to 4017	45.	0.45	2.
Potato	1 Jan to 20 May	233 to 3619	30.	0.45	3.
Field beans	1 Jan to 6 April	always 2184	35.	0.48	4.5
Winter rapeseed	always 1 Jan	451 to 1737	40.	0.5	4.5
Sunflower	25 March to 16 May	1500 to 2800	36.	0.4	3.5

Appendix B: Selected FluxNet Sites Information

In this study, we have used a selection of seven cropland sites located across three key climate zones of Europe (cold, temperate, and Mediterranean) in order to validate the carbon fluxes generated with our optimized model WOFOST-opt. These selected sites are part of a larger data set for micrometeorological flux measurements, called FluxNet (Baldocchi et al., 2001). The selected FluxNet field campaigns used in this study all follow the Tier 1 data policy (i.e., are open and free for scientific purposes but require fair use). For convenience, we summarize key information about them in Table B1.

Table B1
Crop Rotation and Irrigation Information for our Seven FluxNet Sites, From 2001 to 2014

Site ID		Dates			Optimum
(reference paper)	Crop	Sowing	Harvest	Irrigation	f_{gap}
BE-Lon	sugar beet	30 Mar 2004	29 Sep 2004	no	**0.84**
(Moureaux et al., 2006)	winter wheat	14 Oct 2004	Aug 3 2005	no	0.80
	potato	1 May 2006	15 Sep 2006	no	1.00
	winter wheat	13 Oct 2006	5 Aug 2007	no	0.75
	sugar beet	22 Apr 2008	4 Nov 2008	no	0.86
	winter wheat	13 Nov 2008	7 Aug 2009	no	0.80
	potato	25 Apr 2010	5 Sep 2010	no	1.00
	winter wheat	14 Nov 2010	16 Aug 2011	no	0.75
	grain maize	14 May 2012	13 Oct 2012	no	0.70
	winter wheat	25 Oct 2012	12 Aug 2013	no	0.89
	potato	7 Apr 2014	22 Aug 2014	no	**0.69**
DE-Kli	winter barley	6 Sep 2003	31 Jul 2004	no	0.69
(Prescher et al., 2010)	winter rapeseed	18 Aug 2004	20 Aug 2005	no	0.89
	winter wheat	25 Sep 2005	6 Sep 2006	no	**0.92**
	fodder maize	23 Apr 2007	2 Oct 2007	no	1.00
	spring barley	25 Apr 2008	27 Aug 2008	no	0.75
	winter barley	12 Sep 2008	22 Jul 2009	no	0.67
	winter rapeseed	25 Aug 2009	24 Aug 2010	no	0.94
	winter wheat	2 Oct 2010	22 Aug 2011	no	0.67
	fodder maize	25 Apr 2012	19 Sep 2012	no	1.00
	spring barley	17 Apr 2013	24 Aug 2013	no	0.70
	winter barley	1 Oct 2013	20 July 2014	no	0.80
FI-Jok	spring barley	25 May 2001	21 Sep 2001	no	**0.70**
(Lohila et al., 2004)					
FR-Gri	winter barley	16 Oct 2003	2 Jul 2004	no	0.73
(Loubet et al., 2011)	grain maize	9 May 2005	28 Sep 2005	no	1.00
	winter wheat	28 Oct 2005	15 Jul 2006	no	1.00
	winter barley	4 Oct 2006	29 Jun 2007	no	0.77
	grain maize	4 Apr 2008	10 Sep 2008	no	1.00
	winter wheat	17 Oct 2008	31 Jul 2009	no	0.94
	fodder maize	21 Apr 2011	6 Sep 2011	no	1.00
	winter wheat	20 Oct 2011	3 Aug 2012	no	0.73
	winter rapeseed	31 Aug 2012	15 Aug 2013	no	**0.83**
IT-BCi	fodder maize	9 May 2004	26 Aug 2004	yes	**1.00**
(Vitale et al., 2007)	fodder maize	17 May 2005	24 Aug 2005	yes	1.00
	fodder maize	27 Apr 2006	22 Aug 2006	yes	1.00
	fodder maize	9 May 2007	24 Aug 2007	yes	1.00
	fodder maize	30 Apr 2008	22 Aug 2008	yes	1.00

Table B1 *(continued)*

Site ID (reference paper)	Crop	Dates Sowing	Harvest	Irrigation	Optimum f_{gap}
	fodder maize	11 Jun 2009	8 Sep 2009	yes	1.00
NL-Dij (Jans et al., 2010)	fodder maize	5 May 2007	9 Oct 2007	no	0.88
NL-Lan (Moors et al., 2010)	grain maize	18 May 2005	19 Oct 2005	no	1.00

Note. We exclude here periods with crops we do not model, such as mustard (BE-Lon and FR-Gri), triticale (FR-Gri), or managed grass (FI-Jok). The last column presents the scaling factors for each of the site years as computed with our standard method (i.e., using CGMS sowing dates and EUROSTAT yields). We use these factors to compute the optimized runs presented in Figures 5 and 6. Sites years with scaling factors in bold are featured in Figure 5.

Appendix C: Statistics On GPP And TER

Similarly to NEE in Table 2, we computed the R2 and RMSEs on GPP and TER, as presented in Tables C1 and C2. As we discuss in section 5.1, we find for all non-Mediterranean sites that the normalized RMSE (NRMSE = RMSE/observed min-max range) for TER is about half of the NRMSE of GPP and NEE (8% for TER, 16–17% for GPP and NEE, for non-Mediterranean sites). This indicates that most efforts to improve NEE should be concentrated on improving GPP in these regions, which can be done, for example, with a more accurate timing of the growing season. On the other hand, we find higher RMSEs and lower R2 both for GPP and TER at the Mediterranean site. There, most efforts should be concentrated on improving the water-stress representation both for TER (soil respiration) and for GPP (irrigation).

Table C1
Statistics of Three GPP Models: (a) SiBCASA (SIB), (b) the Nonoptimized WOFOST (WOF), and (c) the Optimized WOFOST (OPT) Over 40 Years of FluxNet Measurements (see Tables 1 and B1)

	Number of years	Climates	RMSE on GPP (g_C m^{-2} d^{-1}) SIB	WOF	OPT	R^2 of GPP model (-) SIB	WOF	OPT	Min-Max f_{gap} range
Winter wheat									0.67-1.00
FR-Gri	3	Cfb	3.59	3.83	2.83	0.47	0.84	0.85	
DE-Kli	2	Cfb	2.73	3.44	2.63	0.73	0.90	0.82	
BE-Lon	5	Cfb	4.53	3.04	2.33	0.47	0.91	0.87	
Grain maize									0.70-1.00
FR-Gri	2	Cfb	4.39	5.82	4.93	0.42	0.65	0.75	
BE-Lon	1	Cfb	5.24	5.81	2.05	0.38	0.79	0.92	
NL-Lan	1	Cfb	4.09	6.44	4.43	0.49	0.67	0.72	
Fodder maize									0.88-1.00
IT-BCi	6	Cfa	8.53	11.68	9.67	0.25	0.03	0.03	
FR-Gri	1	Cfb	4.91	5.31	5.29	0.60	0.70	0.68	
DE-Kli	2	Cfb	3.65	8.32	7.65	0.42	0.73	0.76	
NL-Dij	1	Cfb	6.22	5.50	4.40	0.48	0.86	0.91	
Winter barley									0.67-0.80
FR-Gri	2	Cfb	4.19	2.83	2.43	0.23	0.88	0.90	
DE-Kli	3	Cfb	4.21	3.77	2.70	0.35	0.83	0.85	
Spring barley									0.70-0.75
DE-Kli	2	Cfb	3.42	4.02	1.93	0.71	0.85	0.85	
FI-Jok	1	Dfb	3.29	1.96	0.64	0.61	0.93	0.93	

Table C1 *(continued)*

	Number of years	Climates	RMSE on GPP (g_C m^{-2} d^{-1}) SIB	WOF	OPT	R^2 of GPP model (-) SIB	WOF	OPT	Min-Max f_{gap} range
Winter rapeseed									0.83-0.94
FR-Gri	1	Cfb	2.72	3.69	2.18	0.63	0.86	0.85	
DE-Kli	2	Cfb	3.17	4.09	3.42	0.58	0.80	0.79	
Potato									0.69-1.00
BE-Lon	3	Cfb	3.97	3.48	2.44	0.38	0.55	0.67	
Sugar beet									0.84-0.86
BE-Lon	2	Cfb	4.22	3.27	1.66	0.50	0.87	0.94	

Table C2
Statistics of Three TER Models: (a) SiBCASA (SIB), (b) the Nonoptimized WOFOST (WOF), and (c) the Optimized WOFOST (OPT) over 40 Years of FluxNet Measurements (See Tables 1 and B1)

	Number of years	Climates	RMSE on TER (g_C m^{-2} d^{-1}) SIB	WOF	OPT	R^2 of TER model (-) SIB	WOF	OPT	Min-Max f_{gap} range
Winter wheat									0.67-1.00
FR-Gri	3	Cfb	1.56	1.34	1.11	0.60	0.79	0.81	
DE-Kli	2	Cfb	1.85	1.39	1.29	0.67	0.74	0.76	
BE-Lon	5	Cfb	1.92	1.09	0.98	0.58	0.83	0.83	
Grain maize									0.70-1.00
FR-Gri	2	Cfb	2.11	2.31	1.71	0.41	0.42	0.66	
BE-Lon	1	Cfb	3.09	2.86	2.04	0.38	0.44	0.71	
NL-Lan	1	Cfb	2.38	2.29	2.19	0.68	0.67	0.75	
Fodder maize									0.88-1.00
IT-BCi	6	Cfa	3.28	4.45	3.96	0.03	0.13	0.00	
FR-Gri	1	Cfb	1.92	2.25	2.34	0.55	0.45	0.38	
DE-Kli	2	Cfb	2.09	2.49	2.42	0.75	0.66	0.64	
NL-Dij	1	Cfb	1.83	1.76	1.63	0.79	0.72	0.76	
Winter barley									0.67-0.80
FR-Gri	2	Cfb	1.70	1.20	0.95	0.61	0.62	0.64	
DE-Kli	3	Cfb	1.67	1.17	1.21	0.72	0.79	0.88	
Spring barley									0.70-0.75
DE-Kli	2	Cfb	2.77	1.22	0.83	0.70	0.83	0.88	
FI-Jok	1	Dfb	2.24	0.75	0.61	0.80	0.91	0.92	
Winter rapeseed									0.83-0.94
FR-Gri	1	Cfb	1.29	1.80	1.28	0.67	0.65	0.70	
DE-Kli	2	Cfb	1.55	1.50	1.38	0.80	0.76	0.78	
Potato									0.69-1.00
BE-Lon	3	Cfb	2.88	0.99	0.76	0.50	0.73	0.85	
Sugar beet									0.84-0.86
BE-Lon	2	Cfb	2.44	1.36	1.11	0.60	0.82	0.80	

Acknowledgments
The WOFOST-opt code is freely accessible at github.com/mariecombe/pcse.git, on branch "marie." However, a successful installation of the code might require interaction with staff members from our department, namely, Wouter Peters (wouter.peters@wur.nl) or Ingrid van der Laan-Luikkx (ingrid.vanderlaan@wur.nl). This is because partial code developments (e.g., for water stress and postharvest processes) are also uploaded on the Github repository. The input data necessary to run the framework were previously published by Boogaard et al. (2013) (CGMS data) and Dee et al. (2011) (ERA-Interim data). Authorization from the Joint Research Centre (JRC) must be requested to use the CGMS data but is easily granted for scientific purposes. To get this authorization, please contact Hendrik Boogaard (hendrik.boogaard@wur.nl). Finally, the EUROSTAT grain yield data are freely accessible at http://ec.europa.eu/eurostat. This research was funded by the Netherlands Organization for Scientific Research (NWO) through the VIDI grant 864.08.012. This research was also supported by a grant for computing time (SH-312-14) from the Netherlands Organization for Scientific Research (NWO). We claim no conflict of interest. We want to thank Hendrik Boogaard and the Joint Research Centre (JRC) for granting us access to the European crop and soil input data sets of the European Commission's Crop Growth Monitoring System (CGMS). We also want to thank the FluxNet community for giving free access to their Tier 1 data set. In particular, we want to acknowledge the help from Cor Jacobs, Wilma Jans, Eddy Moors, Thomas Grünwald, Benjamin Loubet, Nicolas Mascher, Tanguy Manise, Marc Aubinet, Pauline Buysse, and Anne Deligne, who provided their help to interpret the measurements. We finally acknowledge the help from Ingrid Super and Erik van Schaik for the SiBCASA simulations.

References

Alden, C. B., Miller, J. B., Gatti, L. V., Gloor, M. M., Guan, K., Michalak, A. M., … Diffenbaugh, N. S. (2016). Regional atmospheric CO_2 inversion reveals seasonal and geographic differences in Amazon net biome exchange. *Global Change Biology*, *22*, 3427–3443. https://doi.org/10.1111/gcb.13305

Baldocchi, D., Falge, E., Gu, L., & Olson, R. (2001). FluxNet: A new tool to study the temporal and spatial variability of ecosystem-scale carbon dioxide, water vapor, and energy flux densities. *Bulletin of the American Meteorological Society*, *82*, 2415–2434. https://doi.org/10.1175/1520-0477(2001)082<2415:fantts>2.3.co;2

Bondeau, A., Smith, P. C., Zaehle, S., Schaphoff, S., Lucht, W., Cramer, W., … Smith, B. (2007). Modelling the role of agriculture for the 20th century global terrestrial carbon balance. *Global Change Biology*, *13*, 679–706. https://doi.org/10.1111/j.1365-2486.2006.01305.x

Boogaard, H., Wolf, J., Supit, I., Niemeyer, S., & van Ittersum, M. (2013). A regional implementation of WOFOST for calculating yield gaps of autumn-sown wheat across the European Union. *Field Crops Research*, *143*, 130–142.

Bregaglio, S., Frasso, N., Pagani, V., Stella, T., Francone, C., Cappelli, G., … Confalonieri, R. (2014). New multi-model approach gives good estimations of wheat yield under semi-arid climate in Morocco. *Agronomy for Sustainable Development*, *35*, 157–167. https://doi.org/10.1007/s13593-014-0225-6

Bussay, A., van der Velde, M., Fumagalli, D., & Seguini, L. (2015). Improving operational maize yield forecasting in Hungary. *Agricultural Systems*, *141*, 94–106. https://doi.org/10.1016/j.agsy.2015.10.001

Camargo, G. G. T., & Kemanian, A. R. (2016). Six crop models differ in their simulation of water uptake. *Agricultural and Forest Meteorology*, *220*, 116–129. https://doi.org/10.1016/j.agrformet.2016.01.013

Carbone, M. S., Still, C. J., Ambrose, A. R., Dawson, T. E., Williams, A. P., Boot, C. M., … Schimel, J. P. (2011). Seasonal and episodic moisture controls on plant and microbial contributions to soil respiration. *Oecologia*, *167*, 265–278. https://doi.org/10.1007/s00442-011-1975-3

Chen, J. M., Fung, J. W., Mo, G., Deng, F., & West, T. O. (2015). Atmospheric inversion of surface carbon flux with consideration of the spatial distribution of US crop production and consumption. *Biogeosciences*, *12*, 323–343.

Ciais, P., Bousquet, P., Freibauer, A., & Naegler, T. (2007). Horizontal displacement of carbon associated with agriculture and its impacts on atmospheric CO_2. *Global Biogeochemical Cycles*, *21*, GB2014. https://doi.org/10.1029/2006GB002741

Ciais, P., Borges, A. V., Abril, G., Meybeck, M., Folberth, G., Hauglustaine, D., & Janssens, I. A. (2008). The impact of lateral carbon fluxes on the European carbon balance. *Biogeosciences*, *5*, 1259–1271.

Ciais, P., Wattenbach, M., Vuichard, N., Smith, P., Piao, S. L., Don, A., … Schulze, E. D. (2010). The European carbon balance. Part 2: Croplands. *Global Change Biology*, *16*, 1409–1428.

Combe, M., Vilà-Guerau de Arellano, J., Ouwersloot, H. G., Jacobs, C. M. J., & Peters, W. (2015). Two perspectives on the coupled carbon, water, and energy exchange in the planetary boundary layer. *Biogeosciences*, *12*, 103–123. https://doi.org/10.5194/bg-12-103-2015

Combe, M., Vilà-Guerau de Arellano, J., Ouwersloot, H. G., & Peters, W. (2016). Plant water-stress parameterization determines the strength of land–atmosphere coupling. *Agricultural and Forest Meteorology*, *217*, 61–73. https://doi.org/10.1016/j.agrformet.2015.11.006

Conant, R. T., Dalla-Betta, P., Klopatek, C. C., & Klopatek, J. M. (2004). Controls on soil respiration in semiarid soils. *Soil Biology and Biochemistry*, *36*, 945–951. https://doi.org/10.1016/j.soilbio.2004.02.013

Corbin, K. D., Denning, A. S., Lokupitiya, E. Y., Schuh, A. E., Miles, N. L., Davis, K. J., … Baker, I. T. (2010). Assessing the impact of crops on regional CO_2 fluxes and atmospheric concentrations, Tellus Ser. *B*, *62*, 521–532. https://doi.org/10.1111/j.1600-0889.2010.00485.x

de Noblet-Ducoudré, N., Gervois, S., Ciais, P., Viovy, N., Brisson, N., Seguin, B., & Perrier, A. (2004). Coupling the soil-vegetation-atmosphere-transfer scheme ORCHIDEE to the agronomy model STICS to study the influence of croplands on the European carbon and water budgets. *Agronomie*, *24*, 397–407.

de Wit, A., Baruth, B., Boogaard, H., van Diepen, K., van Kraalingen, D., Micale, F., … van den Wijngaart, R. (2010). Using ERA-Interim for regional crop yield forecasting in Europe. *Climate Research*, *44*, 41–53. https://doi.org/10.3354/cr00872

de Wit, A. J. W., & Van Diepen, C. A. (2007). Crop model data assimilation with the Ensemble Kalman filter for improving regional crop yield forecasts. *Agricultural and Forest Meteorology*, *146*, 38–56.

Dee, D. P., Uppala, S. M., Simmons, A. J., Berrisford, P., Poli, P., Kobayashi, S., … Vitart, F. (2011). The ERA-Interim reanalysis: configuration and performance of the data assimilation system. *Quarterly Journal of the Royal Meteorological Society*, *137*, 553–597. https://doi.org/10.1002/qj.828

Dua, V. K., Singh, B. P., Govindakrishnan, P. M., Kumar, S., & Lal, S. S. (2013). Impact of climate change on potato productivity in Punjab—A simulation study. *Current Science*, *105*, 787–794.

Eitzinger, J., Thaler, S., Schmid, E., Strauss, F., Ferrise, R., & Moriondo, M. (2013). Sensitivities of crop models to extreme weather conditions during flowering period demonstrated for maize and winter wheat in Austria. *Journal of Agricultural Science*, *151*, 813–835.

European Commission (2005). JRC MARS Bulletin (Tech. Rep., Vol. 13, No. 6). Ispra, Italy: JRC.

EUROSTAT (2015). European regional statistics on agriculture, land use, and demography, Online database of the Statistical Office of the European Union. Retrieved from http://ec.europa.eu/eurostat/web/regions/data/database, Last accessed on February 18, 2016.

Foltescu, V. L. (2000). Prediction of crop yield in Sweden based on mesoscale meteorological analysis. *Meteorological Applications*, *7*, 313–321. https://doi.org/10.1017/S1350482700001687

García-Herrera, R., Hernández, E., Barriopedro, D., Paredes, D., Trigo, R. M., Trigo, I. F., & Mendes, M. A. (2007). The outstanding 2004/05 drought in the Iberian Peninsula: Associated atmospheric circulation. *Journal of Hydrometeorology*, *8*, 483–498. https://doi.org/10.1175/JHM578.1

Gouveia, C., Trigo, R. M., & DaCamara, C. C. (2009). Drought and vegetation stress monitoring in Portugal using satellite data. *Natural Hazards and Earth System Sciences*, *9*, 185–195. https://doi.org/10.5194/nhess-9-185-2009

Gray, J. M., Frolking, S., Kort, E. A., Ray, D. K., Kucharik, C. J., Ramankutty, N., & Friedl, M. A. (2014). Direct human influence on atmospheric CO_2 seasonality from increased cropland productivity. *Nature*, *515*, 398–401. https://doi.org/10.1038/nature13957

Hope, C., & Schaefer, K. (2015). Economic impacts of carbon dioxide and methane released from thawing permafrost. *Nature Climate Change*, *6*, 56–59. https://doi.org/10.1038/nclimate2807

Jacobs, C., Jacobs, A., Bosveld, F. C., Hendriks, D., Hensen, A., Kroon, P. S., … Veenendaal, E. M. (2007). Variability of annual CO_2 exchange from Dutch grasslands. *Biogeosciences*, *4*, 803–816. https://doi.org/10.5194/bg-4-803-2007

Jans, W. W. P., Jacobs, C. M. J., Kruijt, B., Elbers, J. A., Barendse, S., & Moors, E. J. (2010). Carbon exchange of a maize (Zea mays L.) crop: Influence of phenology. *Agriculture Ecosystems and Environment*, *139*, 316–324. https://doi.org/10.1016/j.agee.2010.06.008

Kassie, B. T., Van Ittersum, M. K., Hengsdijk, H., Asseng, S., Wolf, J., & Rotter, R. P. (2014). Climate-induced yield variability and yield gaps of maize (Zea mays L.) in the Central Rift Valley of Ethiopia. *Field Crops Research*, *160*, 41–53. https://doi.org/10.1016/j.fcr.2014.02.010

Kogan, F., Kussul, N., Adamenko, T., Skakun, S., Kravchenko, O., Kryvobok, O., … Lavrenyuk, A. (2013). Winter wheat yield forecasting in Ukraine based on Earth observation, meteorological data and biophysical models. *International Journal of Applied Earth Observations and Geoinformation*, *23*, 192–203. https://doi.org/10.1016/j.jag.2013.01.002

Kothavala, Z., Arain, M. A., Black, T. A., & Verseghy, D. (2005). The simulation of energy, water vapor and carbon dioxide fluxes over common crops by the Canadian Land Surface Scheme (CLASS). *Agricultural And Forest Meteorology*, *133*, 89–108.

Krinner, G., Viovy, N., De Noblet-Ducoudré, N., Ogée, J., Polcher, J., & Friedlingstein, P. (2005). A dynamic global vegetation model for studies of the coupled atmosphere-biosphere system. *Global Biogeochemical Cycles*, *19*, GB1015. https://doi.org/10.1029/2003GB002199

Kutsch, W. L., Aubinet, M., Buchmann, N., Smith, P., Osborne, B., Eugster, W., … Ziegler, W. (2010). The net biome production of full crop rotations in Europe. *Agriculture Ecosystems and Environment*, *139*, 336–345.

Lal, R. (2004). Soil carbon sequestration impacts on global climate change and food security. *Science*, *304*, 1623–1627.

Le Quéré, C., Moriarty, R., Andrew, R. M., Canadell, J. G., Sitch, S., Korsbakken, J. I., & Zeng, N. (2015). Global carbon budget 2015. *Earth System Science Data*, *7*, 349–396. https://doi.org/10.5194/essd-7-349-2015

Li, Y., Zhou, J., Kinzelbach, W., Cheng, G., Li, X., & Zhao, W. (2013). Coupling a SVAT heat and water flow model, a stomatal-photosynthesis model and a crop growth model to simulate energy, water and carbon fluxes in an irrigated maize ecosystem. *Agricultural and Forest Meteorology*, *176*, 10–24. https://doi.org/10.1016/j.agrformet.2013.03.004

Lloyd, J., & Taylor, J. A. (1994). On the temperature dependence of soil respiration. *Functional Ecology*, *8*, 315–323. https://doi.org/10.2307/2389824

Lohila, A., Aurela, M., Tuovinen, J.-P., & Laurila, T. (2004). Annual CO_2 exchange of a peat field growing spring barley or perennial forage grass. *Journal of Geophysical Research*, *109*, D18116. https://doi.org/10.1029/2004JD004715

Lokupitiya, E., Denning, S., Paustian, K., Baker, I., Schaefer, K., Verma, S., … Fischer, M. (2009). Incorporation of crop phenology in Simple Biosphere Model (SiBcrop) to improve land-atmosphere carbon exchanges from croplands. *Biogeosciences*, *6*, 969–986.

Lokupitiya, E., Denning, A. S., Schaefer, K., Ricciuto, D., Anderson, R., Arain, M. A., … Xue, Y. (2016). Carbon and energy fluxes in cropland ecosystems: A model-data comparison. *Biogeochemistry*, *129*, 1–26.

Loubet, B., Laville, P., Lehuger, S., Larmanou, E., Fléchard, C., Mascher, N., … Cellier, P. (2011). Carbon, nitrogen and Greenhouse gases budgets over a four years crop rotation in northern France. *Plant and Soil*, *343*, 109–137. https://doi.org/10.1007/s11104-011-0751-9

Moors, E. J., Jacobs, C., Jans, W., Supit, I., Kutsch, W. L., Bernhofer, C., … Soegaard, H. (2010). Variability in carbon exchange of European croplands. *Agriculture, Ecosystems and Environment*, *139*, 325–335. https://doi.org/10.1016/j.agee.2010.04.013

Moureaux, C., Debacq, A., Bodson, B., Heinesch, B., & Aubinet, M. (2006). Annual net ecosystem carbon exchange by a sugar beet crop. *Agricultural and Forest Meteorology*, *139*, 25–39.

Moyano, F. E., Manzoni, S., & Chenu, C. (2013). Responses of soil heterotrophic respiration to moisture availability: An exploration of processes and models. *Soil Biology and Biochemistry*, *59*, 72–85. https://doi.org/10.1016/j.soilbio.2013. 01.002

Pan, Y., Birdsey, R. A., Fang, J., & Houghton, R. (2011). A large and persistent carbon sink in the world's forests. *Science*, *333*, 988–993. https://doi.org/10.1126/science.1201609

Peel, M. C., Finlayson, B. L., & McMahon, T. A. (2007). Updated world map of the Köppen-Geiger climate classification. *Hydrology and Earth System Sciences*, *11*, 1633–1644. https://doi.org/10.5194/hess-11-1633-2007

Peltonen-Sainio, P., Jauhiainen, L., Palosuo, T., Hakala, K., & Ruosteenoja, K. (2015). Rainfed crop production challenges under European high-latitude conditions. *Regional Environmental Change*, *16*, 1521–1533. https://doi.org/10.1007/s10113-015-0875-1

Peters, W., Krol, M. C., van der Werf, G. R., Houweling, S., Jones, C. D., Hughes, J., … Tans, P. P. (2010). Seven years of recent European net terrestrial carbon dioxide exchange constrained by atmospheric observations. *Global Change Biology*, *16*, 1317–1337.

Pingali, P. L. (2012). Green Revolution: Impacts, limits, and the path ahead. *Proceedings of the National Academy of Sciences of the United States of America*, *109*, 12302–12308. https://doi.org/10.1073/pnas.0912953109

Prescher, A.-K., Grunwald, T., & Bernhofer, C. (2010). Land use regulates carbon budgets in eastern Germany: From NEE to NBP. *Agricultural and Forest Meteorology*, *150*, 1016–1025. https://doi.org/10.1016/j.agrformet.2010.03.008

Ramankutty, N., Foley, J. A., & Olejniczak, N. J. (2002). People on the land: Changes in global population and croplands during the 20th century. *AMBIO: A Journal of the Human Environment*, *31*, 251–527. https://doi.org/10.1639/0044-7447(2002) 031[0251:potlci]2.0.co;2

Reichstein, M., Falge, E., Baldocchi, D., Papale, D., Aubinet, M., Berbigier, P., … Valentini, R. (2005). On the separation of net ecosystem exchange into assimilation and ecosystem respiration: Review and improved algorithm. *Global Change Biology*, *11*, 1424–1439. https://doi.org/10.1111/j.1365-2486.2005.001002.x

Richardson, A. D., Anderson, R. S., Arain, M. A., Barr, A. G., Bohrer, G., Chen, G., … Xue, Y. (2011). Terrestrial biosphere models need better representation of vegetation phenology: Results from the North American Carbon Program Site Synthesis. *Global Change Biology*, *18*, 566–584. https://doi.org/10.1111/j.1365-2486.2011.02562.x

Roberts, L. (2011). 9 Billion? *Science*, *333*, 540–543. https://doi.org/10.1126/science.333.6042.540

Sargordi, F., Bansouleh, B. F., Sharifi, M. A., & Van Keulen, H. (2013). Spatio-temporal variation of wheat and silage maize water requirement using CGMS model. *International Journal of Plant Production*, *7*, 207–224.

Schaefer, K., Collatz, G. J., Tans, P., Denning, A. S., Baker, I., Berry, J., … Philpott, A. (2008). Combined simple biosphere/Carnegie-Ames-Stanford approach terrestrial carbon cycle model. *Journal of Geophysical Research*, *113*, G03034. https://doi.org/10.1029/2007JG000603

Scheid, F. (1968). *Gaussian integration*.

Smith, P., Bustamante, M., Ahammad, H., Clark, H., Dong, H., Elsiddig, E. A., … Tubiello, F. (2014). Agriculture, forestry and other land use (AFOLU). In O. Edenhofer et al. (Eds.), *Climate Change 2014: Mitigation of Climate Change* (pp. 811–922). Cambridge, UK: Cambridge University Press.

Spinoni, J., Naumann, G., Vogt, J. V., & Barbosa, P. (2015). The biggest drought events in Europe from 1950 to 2012. *Journal of Hydrology: Regional Studies*, *3*, 509–524. https://doi.org/10.1016/j.ejrh.2015.01.001

Supit, I., Hooijer, A. A., & Van Diepen, C. A. (Eds.) (1994). *System description of the WOFOST 6.0 crop simulation model implemented in the CGMS, Theory and Algorithms* (Vol. 1, 144 pp.). Brussels, Luxembourg: European Commission.

Sus, O., Heuer, M. W., Meyers, T. P., & Williams, M. (2013). A data assimilation framework for constraining upscaled cropland carbon flux seasonality and biometry with MODIS. *Biogeosciences*, *10*, 2451–2466.

Tao, S., Shen, S., Li, Y., Wang, Q., Gao, P., & Mugume, I. (2016). Projected crop production under regional climate change using scenario data and modeling: Sensitivity to chosen sowing date and cultivar. *Sustainability*, *8*, 214–23. https://doi.org/10.3390/su8030214

Tolk, L. F., Peters, W., Meesters, A. G. C. A., Groenendijk, M., Vermeulen, A. T., Steeneveld, G. J., & Dolman, A. J. (2009). Modelling regional scale surface fluxes, meteorology and CO_2 mixing ratios for the Cabauw tower in the Netherlands. *Biogeosciences*, *6*, 2265–2280.

van der Laan-Luijkx, I. T., van der Velde, I. R., van der Veen, E., Tsuruta, A., Stanislawska, K., Babenhauserheide, A., … Peters, W. (2017). The CarbonTracker Data Assimilation Shell (CTDAS) v1.0: Implementation and global carbon balance 2001–2015. *Geoscientific Model Development*, *10*, 2785–280. https://doi.org/10.5194/gmd-10-2785-2017

van der Molen, M. K., de Jeu, R. A. M., Wagner, W., van der Velde, I. R., Kolari, P., Kurbatova, J., … Peters, W. (2016). The effect of assimilating satellite-derived soil moisture data in SiBCASA on simulated carbon fluxes in Boreal Eurasia. *Hydrology and Earth System Sciences*, *20*, 605–624. https://doi.org/10.5194/hess-20-605-2016

van der Velde, I. R. (2015). Studying biosphere-atmosphere exchange of CO_2 (PhD thesis). Wageningen, Netherlands: Wageningen University.

van der Velde, I. R., Miller, J. B., Schaefer, K., van der Werf, G. R., Krol, M. C., & Peters, W. (2014). Terrestrial cycling of $^{13}CO_2$ by photosynthesis, respiration, and biomass burning in SiBCASA. *Biogeosciences*, *11*, 6553–6571. https://doi.org/10.5194/bg-11-6553-2014

van Ittersum, M. K., Leffelaar, P. A., Van Keulen, H., Kropff, M. J., Bastiaans, L., & Goudriaan, J. (2003). On approaches and applications of the Wageningen crop models. *European Journal of Agronomy*, *18*, 201–234.

Vitale, L., Di Tommasi, P., Arena, C., Fierro, A., Virzo De Santo, A., & Magliulo, V. (2007). Effects of water stress on gas exchange of field grown Zea mays L in Southern Italy: An analysis at canopy and leaf level. *Acta Physiologiae Plantarum*, *29*, 317–326. https://doi.org/10.1007/s11738-007-0041-6

Wang, T., Lu, C., & Yu, B. (2011). Production potential and yield gaps of summer maize in the Beijing-Tianjin-Hebei Region. *Journal of Geographical Sciences*, *21*, 677–688. https://doi.org/10.1007/s11442-011-0872-3

West, T. O., Bandaru, V., Brandt, C. C., Schuh, A. E., & Ogle, S. M. (2011). Regional uptake and release of crop carbon in the United States. *Biogeosciences*, *8*, 2037–2046.

Wolf, J., Ouattara, K., & Supit, I. (2015). Sowing rules for estimating rainfed yield potential of sorghum and maize in Burkina Faso. *Agricultural and Forest Meteorology*, *214-215*, 208–218. https://doi.org/10.1016/j.agrformet.2015.08.262

Wriedt, G., van der Velde, M., Aloe, A., & Bouraoui, F. (2009a). Estimating irrigation water requirements in Europe. *Journal of Hydrology*, *373*, 527–544. https://doi.org/10.1016/j.jhydrol.2009.05.018

Wriedt, G., van der Velde, M., Aloe, A., & Bouraoui, F. (2009b). A European irrigation map for spatially distributed agricultural modelling. *Agricultural Water Management*, *96*, 771–789. https://doi.org/10.1016/j.agwat.2008.10.012

Wu, X., Vuichard, N., Ciais, P., Viovy, N., De Noblet-Ducoudré, N., Wang, X., … Ripoche, D. (2016). ORCHIDEE-CROP (v0), a new process-based agro-land surface model: model description and evaluation over Europe. *Geoscientific Model Development*, *9*, 857–873. https://doi.org/10.5194/gmd-9-857-2016

Zeng, N., Zhao, F., Collatz, G. J., Kalnay, E., Salawitch, R. J., West, T. O., & Guanter, L. (2014). Agricultural Green Revolution as a driver of increasing atmospheric CO_2 seasonal amplitude. *Nature*, *515*, 394–397. https://doi.org/10.1038/nature13893